Superconductivity from weak repulsion in hexagonal lattice systems

Rahul Nandkishore,[1,2] Ronny Thomale,[3] and Andrey V. Chubukov[4]

[1]*Princeton Center for Theoretical Science, Princeton University, Princeton, New Jersey 08544, USA*
[2]*Department of Physics, Massachusetts Institute of Technology, Cambridge, Massachusetts 02139, USA*
[3]*Theoretische Physik I, Universität Würzburg, am Hubland, 97074 Würzburg, Germany*
[4]*Department of Physics, University of Wisconsin, Madison, Wisconsin 53706, USA*

We analyze the pairing instabilities for fermions on hexagonal lattices (both honeycomb and triangular ones) in a wide range of fermionic densities ranging from van Hove density at which a single large Fermi surface splits into two disconnected Fermi pockets, to a density at which disconnected pockets shrink to Fermi points (half-filling for a honeycomb lattice and full filling for a triangular lattice). We argue that for a generic doping in this range, superconductivity at weak coupling is of Kohn-Luttinger type, and, due to the presence of electronic interactions beyond on-site repulsion, is a threshold phenomenon, with superconductivity emerging only if the attraction generated by the Kohn-Luttinger mechanism exceeds the bare repulsion in some channel. For disconnected Fermi pockets, we predict that Kohn-Luttinger superconductivity, if it occurs, is likely to be f wave. While the Kohn-Luttinger analysis is adequate over most of the doping range, a more sophisticated analysis is needed near van Hove doping. We treat van Hove doping using a parquet renormalization group, the equations for which we derive and analyze. Near this doping level, superconductivity is a universal phenomenon, arising from any choice of bare repulsive interactions. The strongest pairing instability is into a chiral d-wave state ($d + id$). At a truly weak coupling, the strongest competitor is a spin-density-wave instability, however, d-wave superconductivity still wins. Moreover, the feedback of the spin density fluctuations into the Cooper channel significantly enhances the critical temperature over the estimates of the Kohn-Luttinger theory. We analyze renormalization group equations at stronger couplings and find that the main competitor to d-wave superconductivity away from weak coupling is actually ferromagnetism. We also discuss the effect of the edge fermions and show that they are unimportant in the asymptotic weak coupling limit, but may give rise to, e.g., a charge-density-wave order at moderate coupling strengths.

I. INTRODUCTION

Understanding the instabilities of Fermi liquids has been an enduring theme of research in condensed matter physics for decades [1]. All rotationally isotropic Fermi liquids display an instability to superconductivity in some nonzero angular momentum channel [2–4]. This condition does not hold for nonisotropic Fermi systems, which may remain in the normal state down to $T = 0$. On the other hand, if a lattice system has an attractive interaction in some pairing channel, it may get enhanced when, e.g., the Fermi surface (FS) is nested. The energy scale for superconductivity can also be enhanced by divergences in the FS density of states at certain doping levels.

Of particular interest are situations where a Fermi liquid instability to superconductivity is driven purely by an electron-electron interaction rather than interaction with phonons. This line of research has a long history. Pairing due to direct fermion-fermion interactions was discussed in connection with the superfluidity of ^{3}He [5,6] and became mainstream after the discovery of high-temperature superconductivity in the cuprates [7,8] and subsequent discovery of superconductivity in Fe-based pnictides [9].

The weak coupling scenario of the pairing due to nominally repulsive Coulomb interaction is generally known as the Kohn-Luttinger (KL) mechanism, developed in 1965 (Refs. [2,10]). The KL mechanism is based upon two fundamental earlier results. It was discovered by Friedel [11] in the early 1950s that the screened Coulomb potential in a Fermi liquid has a long-range oscillatory tail $\cos(2k_F r + \phi_0)/r^3$ at large distances

r, hence at some large enough r, the screened Coulomb interaction gets overscreened and becomes attractive. Next, Landau and Pitaevskii analyzed the pairing in an isotropic Fermi liquid at nonzero orbital momentum l of the pair and found that the pairing problem decouples between different l. Because of this decoupling, if only one partial component of the interaction is attractive and all others are repulsive, the system already undergoes a pairing instability into a state with l for which the interaction is attractive [12].

Because the components of the interaction with large l come from large distances, it is conceivable that occasional overscreening of the Coulomb interaction at large distances may make some of the partial interaction components with large l attractive. KL analyzed the form of the fully screened irreducible pairing interaction at large l in three-dimensional, rotationally isotropic systems with $k^2/(2m)$ dispersion, by separating nonanalytic $2k_F$ screening and regular screening from other momenta. KL incorporated the latter into the effective interaction $U(\mathbf{q}) = U(q)$ ($q = |\mathbf{q}|$) and made no assumptions about the form $U(q)$ except that it is an analytic function of q^2. The full irreducible pairing interaction is $U(q)$ plus extra terms coming from the screening (see Fig. 1). An analysis of this form was first performed for the s-wave channel in [13]. KL extended the analysis to nonzero l. They argued that at large l contributions to partial components of the irreducible interaction from $2k_F$ scattering scale as $1/l^4$ due to the nonanalyticity of the $2k_F$ screening (this is the same nonanalyticity which gives rise to Friedel oscillations). At the same time, partial components of analytic $U(q)$ behave
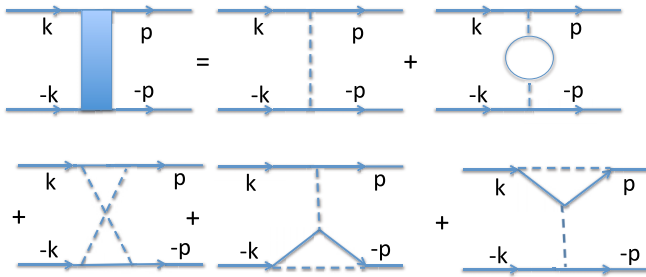
FIG. 1. (Color online) Kohn-Luttinger mechanism of the pairing. The irreducible pairing interaction is the sum of the Coulomb interaction, which includes all regular contribution from screening [$U(q)$, represented by a dashed line], and nonanalytic terms, which appear at second order in $U(q)$. Kohn and Luttinger demonstrated that for rotationally isotropic systems, the partial components of the irreducible pairing interaction are attractive for arbitrary $U(q)$ for large values of the angular momentum l, at least for odd l.

at large l as e^{-l}, i.e., are much smaller. As a result, even though the KL contribution is second order in U, it overwhelms the direct first-order interaction term in channels with large enough l. KL explicitly computed [2,10] the prefactor for the $1/l^4$ term and found that it generally depends on the parity of l. They found that the interaction in channels with odd l is attractive no matter what is the form of $U(q)$. For the highly-screened Hubbard interaction, for which $U(0) = U(2k_F) = U$, the prefactor is attractive for both even and odd l. As a result, any generic rotationally invariant system with repulsive Coulomb interaction is unstable against pairing in channels with sufficiently large l. The pairing will be into a channel that has the largest attractive component. The situation away from the asymptotic large l limit is less certain as the analytic and nonanalytic contributions to the irreducible pairing interaction are of the same order. However, one can make progress if the bare interaction $U(q)$ is weak, by doing perturbation theory in weak interactions. For momentum-independent $U(q) = U$ and an isotropic system, the KL mechanism generates an attraction in all channels down to $l = 1$, with the $l = 1$ channel having the strongest attraction [14,15]. For a momentum-dependent interaction, $U(q)$ itself has components for all l and whether the second-order KL contribution can overwhelm the bare interaction depends on the details [4,16,17].

The situation in lattice systems is similar but not identical to that in isotropic systems. Namely, there is only a discrete set of orthogonal channels imposed by a specific lattice symmetry. (For 2D systems with C_4 lattice symmetry, there are four one-dimensional channels A_{1g}, B_{1g}, B_{2g}, and A_{2g}, and one two-dimensional E_g channel.) Each channel has an infinite set of eigenfunctions. The leading eigenfunctions in each channel can be formally associated with s wave (A_{1g}), p wave (E_g), d wave (B_{1g} and B_{1g}), etc., however, the "higher-momentum" eigenfunctions have the same lattice symmetry as a leading component in one of the channels and just fall into one of the orthogonal subsets. For example, on a lattice with a threefold rotation symmetry, gap functions of the form $\cos \phi$, $\cos 4\phi$, $\cos 7\phi$, ... have the same eigenvalue under threefold rotation and thus belong to the same representation. Moreover, since these gap functions all have the same eigenvalue under

threefold rotation they are not necessarily orthogonal to each other, since the gap magnitude also depends on ϕ (albeit with threefold symmetry). As a result, the notation of a single large l channel no longer exists. (For a detailed discussion of hexagonal lattice representations and its association with superconducting orders see, e.g., Ref. [18]). There is an infinite number of orthogonal linear combinations of eigenfunctions in each subset, hence an infinite number of eigenvalues, and for superconductivity only one of the eigenvalues needs to be attractive. However, there is no generic condition that there must be attractive channels, and, moreover, even if some combinations of eigenfunctions are attractive, there is no condition like in the isotropic case at large l, that the bare interaction $U(q)$ has to be vanishingly small in one of these channels. All this makes the analysis of the pairing in lattice systems more involved than in the isotropic case.

There are two ways to proceed and we explore both. First, in a system with a generic FS (FS) (i.e., the one without nesting and/or special points where the density of state diverges), one can apply perturbation theory and study KL-type superconductivity for a generic $U(r)$. For 2D systems on a tetragonal lattice, such analyses have been performed both analytically and numerically in Refs. [16,17] (see also Ref. [19]). Here, we analyze KL superconductivity analytically for systems on a hexagonal lattice. We show that the subset of potential superconducting states is larger for fermions on a hexagonal lattice than on a tetragonal lattice. We perform a KL-type calculation for a system with an interaction $U(r)$, which is largest on-site (Hubbard component) but also extends to nearest and second-nearest neighbors. We show that the effective interaction taken to second order in the Hubbard U gives rise to an attraction in a d-wave channel near van Hove density and in a channel, which we identify as f wave, in a range of dopings when the FS consists of six disconnected pockets. This result agrees with the numerical analysis in Ref. [20]. Our study provides analytical understanding of the physics of the attraction. (We also consider pairing states not analyzed in Ref. [20]). However, whether or not such superconductivity is actually realized depends on how strong the bare repulsive interaction is in the corresponding channel. For the Hubbard-only model, the bare interaction vanishes for all non-s-wave channels, but for a generic $U(r)$, it is nonzero in all channels. We found that the bare interaction, taken to second neighbors, vanishes in some pairing channels, however, these channels are not the ones in which KL interaction is attractive. As a result, KL attraction (which is second order in the bare coupling) competes with the bare repulsive interaction and must exceed it, otherwise superconductivity would not develop. This implies that superconductivity at a generic doping is a threshold phenomenon: it does not occur if the interaction $U(r)$ is too weak. A somewhat richer behavior can be obtained in multilayer hexagonal lattice systems [21,22], but we do not discuss these here.

Second, at van Hove doping, the density of states diverges at the so-called van Hove points, and, for hopping between nearest neighbors, the FS consists of a set of parallel lines (nesting) (see Fig. 2). In this situation, the KL renormalization of the bare pairing interaction is by itself logarithmically singular and has to be treated on equal footing with the pairing
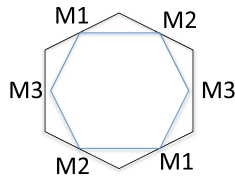
FIG. 2. (Color online) Fermi surface (blue lines) for fermions on a honeycomb lattice at van Hove doping ($\nu = 3/8$ or $5/8$, where $\nu = 1/2$ corresponds to half-filling, where the fermionic spectrum has Dirac points). For nearest-neighbor hopping, the Fermi surface consists of parallel pieces (nesting). At the end point of parallel pieces the density of states diverges (van Hove points M_1, M_2, and M_3). Thin solid lines represent the boundaries of the Brillouin zone.

channel. Moreover, there are logarithmic divergences in channels corresponding to particle-hole pairing [23], which also feed back into the particle-particle pairing channel and may generate additional attraction or repulsion. In this particular case, one can extend the analysis beyond second order in $U(r)$. The analytical technique to do this is called parquet RG [24]. The physics captured by parquet renormalization group (RG) analysis is that KL renormalization gets stronger as one progressively includes higher-order scattering events. The parquet RG equations have been solved in a leading logarithmical approximation in Ref. [25] and the net result for superconductivity can be physically interpreted such that the total pairing interaction (the bare one plus the KL part) evolves as the temperature gets lowered and changes from a repulsive one to an attractive one at some T (in other words, the system self-generates the scale, which is analogous to a Debye frequency). As T further decreases, the attraction grows, and at some lower T the system undergoes a superconducting instability towards a chiral $d + id$ superconducting state which breaks time-reversal symmetry. Note that at van Hove doping, the instability is not a threshold phenomenon but rather occurs for arbitrarily weak bare interactions.

There is a caveat. In a situation when the FS has van Hove points and the interactions flow as T is lowered, superconductivity is not the only one option: the system can also develop a density-wave instability [in this case a spin-density wave (SDW)]. It is known that superconductivity

and SDW do not co-exist [26]. At weak coupling [small bare $U(r)$] and exactly at van Hove density, superconductivity wins over SDW (see Fig. 3). What happens at larger couplings and/or slightly away from van Hove density is less clear, and has been debated in Refs. [18,27–30]. One possibility is that the SDW may win as it wins at intermediate temperature scales, and a deviation from a van Hove density restricts the applicability of RG analysis to temperatures larger than some cutoff. However, to properly address this issue one needs to analyze the set of RG equations beyond the leading logarithmic approximation. This is what we will do in the second part of this paper. We show that at the van Hove point, the physics is highly universal at weak coupling, and the system invariably ends up in a $d + id$ superconducting state. Once we move away from weak coupling, the RG approach is no longer controlled, and the neglect of higher loop diagrams can no longer be justified. However, the procedure can still be applied, although the results must be treated with caution. We show that away from weak coupling the RG analysis that focuses purely on the hexagon corners reveals two distinct instabilities: one to d-wave superconductivity and another to ferromagnetism. The SDW is never the leading instability if the RG is allowed to run indefinitely, but it may dominate if the RG is stopped at some intermediate energy scale by higher loop effects or self-energy effects. The ferromagnetic phase is the principal new result from extending the parquet RG to strong coupling. We also discuss the effect at strong coupling of fermions near the Fermi surface but well away from the van Hove points (referred to henceforth as "edge fermions" because they are near the edges of the hexagonal FS, but are well away from the van Hove points at the corners of the hexagonal FS). Along the ferromagnetic trajectory, the edge fermions suppress ferromagnetism, and may destabilize it in the strong coupling limit towards a different phase, like a charge-density-wave (CDW) or an s-wave superconductor. Meanwhile, along the d-wave superconducting trajectory, the edge fermions strengthen d-wave superconductivity with respect to SDW, but they may destabilise $d + id$ state at strong coupling towards another phase, such as a CDW.

The paper is organized as follows. In the next two sections, we consider KL pairing outside the immediate vicinity of the van Hove density. In Sec. II, we consider fermions on a triangular lattice, and in Sec. III, we consider fermions on a honeycomb lattice. In both cases, we first introduce appropriate patch models and discuss the potential pairing symmetries. We then obtain the bare pairing interaction in various channels for a $U(r)$, which extends to second neighbors. After that, we compute the second-order KL component of the pairing interaction and analyze the full pairing vertices, which consist of first-order terms and second-order KL contributions. We argue that on both lattices a nodeless f-wave pairing is favorable between van Hove density and full filling (triangular lattice) and half-filling (honeycomb lattice), and chiral d-wave ($d + id$) pairing is favorable at and very near van Hove density. In Sec. IV, we discuss the behavior *at* the van Hove density. At this point the superconducting and spin density wave channels mix, so the system is described by a "parquet RG," which we present. Our discussion follows [25], but is substantially more detailed, and we also extend the RG analysis to moderately strong coupling. In Sec. V, we discuss the experimental
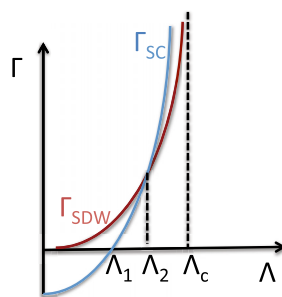

FIG. 3. (Color online) The flow of the couplings in the s-wave superconducting (SC) channel and spin-density-wave (SDW) channel under parquet RG at van Hove density. The SDW coupling wins at intermediate scales. The SC coupling is initially repulsive, but changes sign under RG flow and eventually wins over the coupling in the SDW channel.
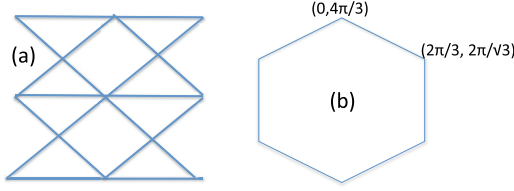
FIG. 4. (Color online) Triangular lattice (a) and the corresponding Brillouin zone in momentum space (b).

situation mostly focusing on doped graphene. We present our conclusions in Sec. VI.

II. SYSTEMS ON A TRIANGULAR LATTICE

A. Fermi surface and fermionic dispersion

Consider a system of fermions on a triangular lattice [Fig. 4(a)] with hopping t between nearest neighbors. The Hamiltonian of free fermions is, in momentum space,

$$\mathcal{H}_2 = \sum_k \varepsilon_k c_k^\dagger c_k, \qquad (1)$$

where

$$\varepsilon_k = -4t \cos \frac{k_x}{2} \left(\cos \frac{k_x}{2} + \cos \frac{k_y \sqrt{3}}{2} \right) - \mu, \qquad (2)$$

and we set the interatomic spacing a to one. The Brillouin zone (BZ) is a hexagon with corner points at $(\pm 4\pi/3, 0)$ and $(\pm 2\pi/3, 2\pi/\sqrt{3})$ [Fig. 4(b)].

The topology of the FS (FS) depends on the value of the chemical potential μ. At $\mu < -8t$ all states are empty at $T = 0$. At $\mu = -8t + \delta$, a small, near-circular FS opens up at the center of the BZ [Fig. 5(a)]. As the chemical potential gets smaller, the area of the FS increases and its shape changes [Fig. 5(b)]. When $\mu = 0$, the FS touches the BZ boundary at six van Hove points $(0, \pm 2\pi/\sqrt{3})$ and

$(\pm \pi, \pm \pi/\sqrt{3})$ [Fig. 5(c)]. Simultaneously, the FS between any nearest van Hove points becomes a straight line, i.e., the FS contains parallel pieces (nesting) Once μ becomes positive, the formerly singly connected FS decouples into 6 disconnected pockets centered at the corners of the BZ [Fig. 5(d)]. At $\mu = t$, the six FSs shrink to points at the BZ boundary at $(\pm \frac{4\pi}{3}, 0)$ and $(\pm \frac{2\pi}{3}, \pm \frac{3\pi}{\sqrt{3}})$.

The van Hove points survive even if the hopping extends beyond nearest neighbors. However, a flat FS acquires a finite curvature once the hopping between second neighbors is added (see also Ref. [18]).

B. The pairing interaction

Throughout this paper we assume that the bare interaction between low-energy fermions is some short-range interaction $U(q)$, i.e., consider the interacting part of the Hamiltonian in the form

$$\mathcal{H}_{\text{int}} = -\frac{1}{2} \sum U_{\alpha,\beta;\gamma,\delta}(k_1, k_2; k_3, k_4) a_{k_1,\alpha}^\dagger a_{k_2,\beta}^\dagger a_{k_3,\gamma} a_{k_4,\delta}, \quad (3)$$

where

$$U_{\alpha,\beta;\gamma,\delta}(k_1, k_2; k_3, k_4) = U(k_1 - k_3) \delta_{\alpha\gamma} \delta_{\beta\delta}, \qquad (4)$$

where $\alpha, \beta, \gamma, \delta$ are spin indices. We will not make any particular assumption about the form of $U(q)$, i.e., will not discuss how it is obtained from the original Coulomb repulsion, except that we assume that $U(q)$ is analytic and is largest at $q = 0$. In an RG sense, $U(q)$ can be understood as the effective four-fermion static interaction, obtained after integrating out high-energy fermions with energies between the bandwidth W and Λ, which is the fraction of the bandwidth, and which sets the upper energy cutoff for our low-energy theory. The screening by high-energy fermions does not give rise to nonanalyticities, hence it is safe to consider $U(q)$ as an analytic function of q. We further assume that $U(q)$ is small compared to Λ and study pairing within perturbation theory (not necessarily lowest order).

An instability in a particular pairing channel manifests itself through the appearance of a pole at zero frequency in the corresponding component of the vertex function $\Gamma_{\alpha,\beta;\gamma,\delta}(k_1, k_2; k_3, k_4)$, which describes two-particle collective bosonic excitations in a system of interacting fermions. The vertex function incorporates multiple fermion-fermion scattering processes at energies below Λ, as well as the Pauli principle, and constitutes the fully renormalized and antisymmetrized four-fermion interaction (Fig. 6). We first consider the pairing interaction to first order in U and then add U^2 terms, which will account for Kohn-Luttinger physics.
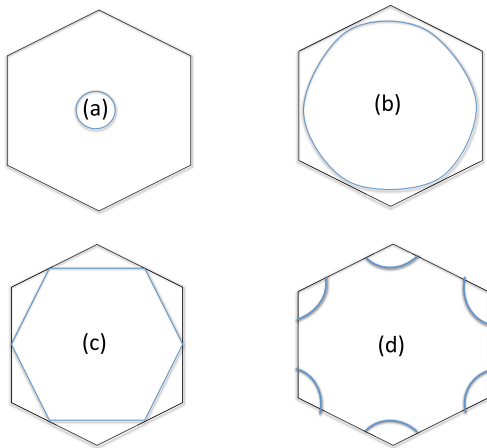

FIG. 5. (Color online) Evolution of the FS with doping for fermions on a triangular lattice: (a) μ slightly above $-8t$, (b) μ approaching zero, (c) $\mu = 0$. This is van Hove doping. The FS consists of parallel pieces, which end at van Hove points where the density of states diverges. (d) $\mu < t$. The FS consists of disconnected pieces.
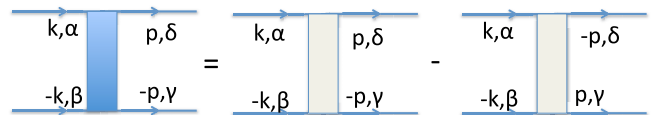

FIG. 6. (Color online) The vertex function, whose poles determine the pairing instability, is the fully renormalized and antisymmetrized interaction at zero total incoming and outgoing momenta.

C. First order in $U(q)$

To first order in $U(q)$, the vertex function coincides with the antisymmetrized interaction

$$\Gamma_{\alpha,\beta;\gamma,\delta}(k_1,k_2;k_3,k_4) = \tfrac{1}{2}[U(k_1-k_3)\delta_{\alpha\gamma}\delta_{\beta\delta}$$
$$- U(k_1-k_4)\delta_{\alpha\delta}\delta_{\beta\gamma}]. \quad (5)$$

At weak coupling, the leading pairing instability occurs at zero total momentum of a pair, and we set $k_1 = -k_2 = k$ and $k_3 = -k_4 = k'$. The part of Γ responsible for the pairing is then

$$\Gamma_{\alpha,\beta;\gamma,\delta}(k,k') = \tfrac{1}{2}[U(k-k')\delta_{\alpha\gamma}\delta_{\beta\delta} - U(k+k')\delta_{\alpha\delta}\delta_{\beta\gamma}]. \quad (6)$$

The vertex function can be further decoupled into spin-singlet and spin-triplet channels as

$$\Gamma_{\alpha,\beta;\gamma,\delta}(k,k') = \tfrac{1}{4}\{[U(k-k') - U(k+k')](\delta_{\alpha\gamma}\delta_{\beta\delta}$$
$$+ \delta_{\alpha\delta}\delta_{\beta\gamma}) + [U(k-k') + U(k+k')](\delta_{\alpha\gamma}\delta_{\beta\delta}$$
$$- \delta_{\alpha\delta}\delta_{\beta\gamma})\}. \quad (7)$$

We now make use of the identities

$$\sum_{\gamma\delta}(\delta_{\alpha\gamma}\delta_{\beta\delta} - \delta_{\alpha\delta}\delta_{\beta\gamma})(\delta_{\gamma\eta}\delta_{\delta\xi} - \delta_{\delta\eta}\delta_{\gamma\xi}) = 2(\delta_{\alpha\eta}\delta_{\beta\xi} - \delta_{\alpha\xi}\delta_{\beta\eta}),$$

$$\sum_{\gamma\delta}(\delta_{\alpha\gamma}\delta_{\beta\delta} + \delta_{\alpha\delta}\delta_{\beta\gamma})(\delta_{\gamma\eta}\delta_{\delta\xi} + \delta_{\delta\eta}\delta_{\gamma\xi}) = 2(\delta_{\alpha\eta}\delta_{\beta\xi} + \delta_{\alpha\xi}\delta_{\beta\eta}),$$

$$(8)$$

to see that the singlet component of $\Gamma_{\alpha,\beta;\gamma,\delta}(k,k')$ determines the pairing instability in the spin-singlet channel with order parameter $\Delta_{\alpha,\beta}(k) = i\sigma^y_{\alpha\beta}\Delta(k)$, and the triplet component of $\Gamma_{\alpha,\beta;\gamma,\delta}(k,k')$ determines the pairing instability in the spin-triplet channel with order parameter $\Delta_{\alpha,\beta}(k) = i\sigma^y_{\alpha\gamma}\sigma_{\gamma\beta} \cdot \mathbf{d}(\mathbf{k})\Delta(k)$, where $\mathbf{d}(k)$ is a unit vector that determines the orientation of the triplet order parameter [31]. For definiteness, we set $\mathbf{d}(k)$ to be antiparallel to z axis, then in the spin-triplet channel $\Delta_{\alpha,\beta}(k) = \sigma^x_{\alpha\beta}\Delta(k)$ (see Fig. 7).

Accordingly, we introduce

$$\Gamma^s = \tfrac{1}{2}[U(k-k') + U(k+k')],$$
$$\Gamma^t = \tfrac{1}{2}[U(k-k') - U(k+k')]. \quad (9)$$

In rotationally invariant systems, each of these two interactions can be further decoupled into orthogonal partial harmonics with either even angular momentum (for Γ^s) or odd angular momentum (for Γ^t). For lattice systems with noncircular FS, such decoupling is impossible and the maximum one can do is to decouple the interaction into a discrete set of representations for the corresponding space group. The components from different sets are orthogonal to each other,
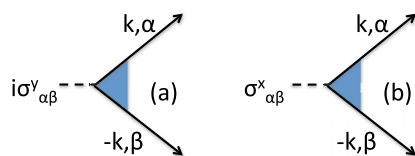
but each set still contains an infinite number of eigenfunctions which are not orthogonal and do not decouple when we solve for superconducting T_c.

Such decoupling into different discrete sets turns out to be useful when all parts of the FS contribute about equally to the pairing. Although all eigenfunctions in each subset are technically of the same order, it turns out that the first harmonics contribute most, such that one can truncate the expansion by keeping only the lowest order terms, e.g., $\cos k_x - \cos k_y$ for d-wave pairing in the cuprates or $a \pm b\cos 2\theta$ for the gaps on electron pockets in Fe pnictides. For fermions on a triangular lattice and μ near zero, the problem, however, is different because the density of states along the FS is maximized near van Hove points, which then play the dominant role in the pairing (just like hot spots play the dominant role in the weak coupling description of the cuprates). If one attempts to compare the contribution to the full Γ from different eigenfunctions from the same subset, one finds that they all contribute nearly equally near such a "van Hove" filling.

In this situation, it is advantageous to use a different approach and restrict the pairing problem to a discrete set of patches where the density of states is the largest and the dimensional coupling constant is the largest (see Figs. 8 and 9). This is the approach which we take in this paper. For fermions on a triangular lattice and near $\mu = 0$, the density of states is maximized in the regions near van Hove points. There are six such regions (patches) on the FS (Fig. 8), but only three are independent because the other three are related to the first three by inverting the sign of the momentum, and superconducting order parameters satisfy $\Delta(-k) = \Delta(k)$ for spin-singlet pairing and $\mathbf{d}(-k) = -\mathbf{d}(k)$ for spin-triplet pairing. The three hot regions are all equivalent in the sense that $2\mathbf{k}_F$ for all three points differs by the reciprocal lattice vector and the interaction at momentum $\mathbf{Q}$ connecting any
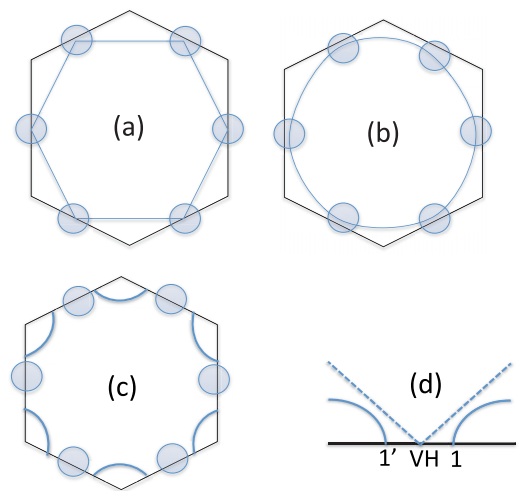
FIG. 8. (Color online) Patch model I assumes that the superconducting gap is concentrated in the shaded patches (a) van Hove doping. The patches are centered at van Hove points: (b) and (c) above and below van Hove doping, respectively; (d) for doping line in (c), the model allows for symmetric and antisymmetric solutions between points 1 and $\bar{1}$.

FIG. 7. (Color online) The pairing vertices for spin-singlet and spin-triplet channels.
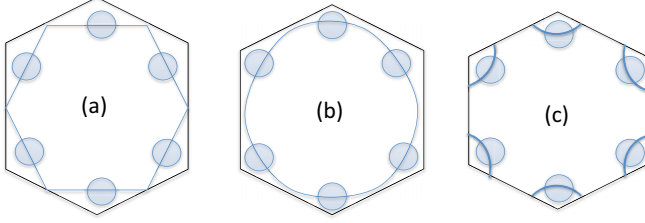
FIG. 9. (Color online) Patch model II. At van Hove doping (a) the patches are centered in between van Hove points: (b) and (c) above and below van Hove doping, respectively. For a FS in the form of disconnected pieces (c), the patches are located at the centers of FS arcs.

two different hot regions is the same $U(|\mathbf{Q}|)$. Accordingly, we define by $U(0)$ the direct interaction within any of the patches, by $U(2k_F)$ the exchange (antisymmetrized) part of intrapatch interaction with momentum transfer from $\mathbf{k}_F$ to $-\mathbf{k}_F$, by $U(Q)$ the direct interaction between patches, and by $U(Q + 2k_F)$ the antisymmetrized part of the interpatch interaction. Because there are intrapatch and interpatch interactions, we introduce two different Γ in either singlet or triplet channel:

$$
\begin{aligned}
\Gamma_s^{(1)} &= \Gamma_s(k,k) = \tfrac{1}{2}[U(0) + U(2k_F)], \\
\Gamma_s^{(2)} &= \Gamma_s(k,k+Q) = \tfrac{1}{2}[U(Q) + U(Q + 2k_F)], \\
\Gamma_t^{(1)} &= \Gamma_t(k,k) = \tfrac{1}{2}[U(0) - U(2k_F)], \\
\Gamma_t^{(2)} &= \Gamma_t(k,k) = \tfrac{1}{2}[U(Q) - U(Q + 2k_F)].
\end{aligned}
\tag{10}
$$

We now introduce three order parameters Δ_i, one for each patch, and solve the 3×3 pairing problem:

$$
\begin{aligned}
\lambda_s \Delta_i &= -\Gamma_s^{(1)} \Delta_i - \Gamma_s^{(2)} \sum_{k \neq i} \Delta_k, \\
\lambda_t \Delta_i &= -\Gamma_t^{(1)} \Delta_i - \Gamma_t^{(2)} \sum_{k \neq i} \Delta_k
\end{aligned}
\tag{11}
$$

for the singlet and triplet channels, respectively. We obtain three eigenfunctions in each channel:

$$
\begin{aligned}
\lambda_s^{(1)} &= -\Gamma_s^{(1)} - 2\Gamma_s^{(2)}, \quad \lambda_s^{(2)} = \lambda_s^{(3)} = -\Gamma_s^{(1)} + \Gamma_s^{(2)}, \\
\lambda_t^{(1)} &= -\Gamma_t^{(1)} - 2\Gamma_t^{(2)}, \quad \lambda_t^{(2)} = \lambda_t^{(3)} = -\Gamma_t^{(1)} + \Gamma_t^{(2)}.
\end{aligned}
\tag{12}
$$

For superconductivity, one needs at least one of these λ to be positive. If all the λ are either negative or zero, the normal state survives down to $T = 0$.

We will label this patch model as model I (Fig. 8). We will also consider another patch model (patch model II), for which we place patches in between van Hove points (see Fig. 9). This second model is less relevant at van Hove filling but it is useful at dopings when the FS splits into six disconnected segments because the patches in the model II are located at the centers of the FS segments.

1. Extended Hubbard model

We apply the results from the previous section to the model with an interaction $U(q)$ which extends up to second neighbors

on a triangular lattice. In momentum space,

$$
\begin{aligned}
U(q) &= U_0 + U_1 \left(\cos q_x + 2 \cos \frac{q_x}{2} \cos \frac{q_y \sqrt{3}}{2} \right) \\
&\quad + U_2 \left(\cos q_y \sqrt{3} + 2 \cos \frac{3q_x}{2} \cos \frac{q_y \sqrt{3}}{2} \right),
\end{aligned}
\tag{13}
$$

where U_0, U_1, and U_2 are amplitudes of the on-site interaction and interaction between first and second neighbors respectively. We assume that $U_0 \gg U_1 \gg U_2$, i.e., that the interaction $U(q)$ rapidly decreases at q comparable to interatomic distances.

Using Eqs. (10)–(13), it is straightforward to obtain eigenfunctions in each of the four channels at various fillings. Because $U(q)$ rapidly drops, we present only the leading contributions to various λ_i (i.e., keep only the largest U_i). We will see, however, that at least in one case, λ_i is only nonzero because of U_2.

a. Van Hove filling, $\mu = 0$. For patch model I, the three patches are centered at $k_1 = (0, -\frac{2\pi}{\sqrt{3}})$, $k_2 = (\pi, \frac{\pi}{\sqrt{3}})$, and $k_3 = (-\pi, \frac{\pi}{\sqrt{3}})$. The other three patches are centered at $-k_i$. One can easily make verify that for each of these k_i, $2k_i \equiv 2k_F$ at van Hove filling coincides with the reciprocal lattice vector. As a result, the eigenfunctions in the spin-triplet channel vanish identically. Meanwhile, in the spin-singlet channel, we have

$$
\lambda_{s,\mathrm{I}}^{(1)} = -3U_0 - U_1 - U_2, \quad \lambda_{s,\mathrm{I}}^{(2)} = \lambda_{s,\mathrm{I}}^{(3)} = -4(U_1 + U_2).
\tag{14}
$$

As long as all interactions are repulsive ($U_j > 0$), both eigenvectors are negative, i.e., both spin-singlet channels are repulsive. Note, however, that if the on site repulsion is the strongest interaction but the first and second-neighbor interactions are attractive (the case of overscreening by high-energy fermions), the system becomes unstable towards d-wave superconductivity.

The structure of the superconducting gap is shown in Fig. 10(a). The eigenfunction $\lambda_s^{(1)}$ corresponds to an s-wave solution (all Δ_i are the same), the eigenfunctions $\lambda_s^{(2)}$ and $\lambda_s^{(3)}$ describe two degenerate solutions, which we call d wave (d_1 and d_2) because if we formally extend the gap to the full FS, we find that for the eigenfunctions corresponding to d_1 and d_2 the gap changes sign four times as one circles the FS. The gaps in the triplet channel vanish identically in patch model I together with eigenvalues $\lambda_{t,\mathrm{I}}^{(i)}$, and we do not show them.

For patch model II, the three patches are centered at $\bar{k}_1 = -(\pi,0)$, $\bar{k}_2 = (\frac{\pi}{2}, \frac{\pi\sqrt{3}}{2})$, and $\bar{k}_3 = (\frac{\pi}{2}, -\frac{\pi\sqrt{3}}{2})$. The couplings are nonzero in both spin-singlet and spin-triplet channels. Setting $U_2 = 0$ for simplicity, we obtain

$$
\begin{aligned}
\lambda_{s,\mathrm{II}}^{(1)} &\approx -3U_0, \quad \lambda_{s,\mathrm{II}}^{(2)} = \lambda_{s,\mathrm{II}}^{(3)} = -U_1, \\
\lambda_{t,\mathrm{II}}^{(1)} &= -4U_1, \quad \lambda_{t,\mathrm{II}}^{(2)} = \lambda_{t,\mathrm{II}}^{(3)} = -U_1.
\end{aligned}
\tag{15}
$$

We see that all bare couplings are repulsive for positive (repulsive) U_0 and U_1.

We show the structure of the superconducting gaps (the eigenfunctions) in all six channels in Fig. 10(b). In the spin-singlet sector, the eigenfunction corresponding to $\lambda_{s,\mathrm{II}}^{(1)}$ is obviously s wave. The eigenfunctions corresponding to
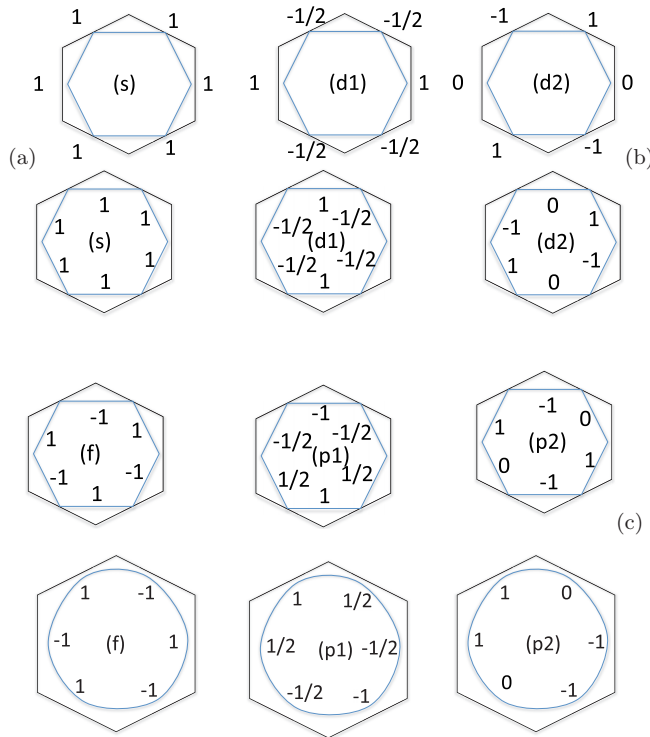
FIG. 10. (Color online) (a) and (b) Structure of the superconducting gap in s-, p-, d-, and f-wave channels at van Hove doping in patch models I and II, respectively. In the p-wave and d-wave channels, the eigenvalues are doubly degenerate. (c) The structure of the gaps in spin-triplet channels in patch model I at $\mu < 0$, when the FS is singly-connected and does not reach van Hove points.

$\lambda_{s,\mathrm{II}}^{(2)} = \lambda_{s,\mathrm{II}}^{(3)}$ again change sign four times as one circles the FS, and we keep calling them d wave. In the spin-triplet sector, the eigenfunction for $\lambda_{t,\mathrm{II}}^{(1)}$ corresponds to an f-wave solution [Δ_i are the same for a triad separated by Q, but each $\Delta_i(-k) = -\Delta_i(k)$], such that the gap changes sign six times as one circles the FS. The eigenfunctions corresponding to $\lambda_{t,\mathrm{II}}^{(2)}$ and $\lambda_{t,\mathrm{II}}^{(3)}$ change sign two times, as one circle the FS, and we label them as p-wave solutions.

b. A smaller filling, $\mu < 0$. We consider relatively small deviations from van Hove filling, at which patch models still make sense (see Fig. 8). For model I, the three patches are now centered at $k_1 = (0, -\frac{2}{\sqrt{3}}(\pi - \delta))$, $k_2 = (\pi - \delta, \frac{\pi-\delta}{\sqrt{3}})$, $k_3 = (-(\pi - \delta), \frac{\pi-\delta}{\sqrt{3}})$, where $\delta \ll 1$ and $\mu \approx -2t\delta^2$. Once δ is nonzero, the couplings in the spin-triplet channel become finite. We have

$$\lambda_{t,\mathrm{I}}^{(1)} = -16U_2\delta^2, \quad \lambda_{s,\mathrm{I}}^{(2)} = \lambda_{s,\mathrm{I}}^{(3)} = -(3U_1 + U_2)\delta^2. \quad (16)$$

As long as U_1 and U_2 are positive (repulsive), the interactions in both spin-triplet channels are repulsive, i.e, spin-triplet superconductivity does not emerge. The interactions in spin-singlet channels were repulsive for $\delta = 0$ (for $U_i > 0$) and remain so at a nonzero positive δ. The structure of the superconducting gaps in spin-singlet channel does not change from Fig. 10(a), but now there appear eigenfunctions in f and p waves, corresponding to the eigenvalues in Eq. (16). We show these eigenfunctions in Fig. 10(c).

For model II (Fig. 9), the patches are centered at $\bar{k}_1 = -(\pi - \bar{\delta}, 0)$, $\bar{k}_2 = (\frac{\pi+\bar{\delta}}{2}, \frac{\sqrt{3}}{2}(\pi + \bar{\delta}))$, $\bar{k}_3 = (\frac{\pi+\bar{\delta}}{2}, -\frac{\sqrt{3}}{2}(\pi + \bar{\delta}))$, and at $-\bar{k}_i$, where $\bar{\delta} = -2\arcsin[(\sqrt{(t-\mu)/t} - 1)/2]$. For $\mu < 0$, $\bar{\delta}$ is negative. The couplings are given by (setting $U_2 = 0$)

$$\lambda_{s,\mathrm{II}}^{(1)} \approx -3U_0,$$

$$\lambda_{s,\mathrm{II}}^{(2)} = \lambda_{s,\mathrm{II}}^{(3)} = -\frac{U_1}{2}[2 + \cos 2\bar{\delta} - \cos \bar{\delta}(1 + 4\sin \bar{\delta}/2)],$$

$$\lambda_{t,\mathrm{II}}^{(1)} = -4U_1\cos^2 \bar{\delta}/2(1 + \sin \bar{\delta}/2)^2, \qquad (17)$$

$$\lambda_{t,\mathrm{II}}^{(2)} = \lambda_{t,\mathrm{II}}^{(3)} = -U_1\cos^2 \bar{\delta}/2(1 - 2\sin \bar{\delta}/2)^2.$$

For $\bar{\delta} = 0$, we reproduce (15). We see that all interactions remain repulsive for arbitrary $\bar{\delta}$, as long as U_0 and U_1 are positive. The structure of the eigenfunctions in s, d, and p channels remains the same as in Fig. 10(b).

c. A larger filling, $\mu > 0$. The situation becomes more interesting at a larger filling, when the FS splits into six pockets, each centered at the corner of the BZ. At small positive $\mu = 2t\delta^2$, one can still focus on patch model I with patches near the van Hove points $(0, -\frac{2\pi}{\sqrt{3}})$, $(\pi, \frac{\pi}{\sqrt{3}})$, and $(-\pi, \frac{\pi}{\sqrt{3}})$, but now each van Hove point splits into two FS points. For example, $k_1 = (0, -\frac{2\pi}{\sqrt{3}})$ splits into $k_{1,+} = (2\delta, -\frac{2\pi}{\sqrt{3}})$ and $k_{1,-} = (-2\delta, -\frac{2\pi}{\sqrt{3}})$. This splitting opens a possibility to consider two types of solutions for the gaps in each patch: a symmetric one, for which $\Delta_{k_{1,+}} = \Delta_{k_{1,-}}$ and antisymmetric one, for which $\Delta_{k_{1,+}} = -\Delta_{k_{1,-}}$. We label the corresponding λ with additional subindices s and a.

A simple analysis shows that the expressions for the vertices in spin-singlet and spin-triplet channels for symmetric and antisymmetric solutions are obtained by replacing in Eq. (10):

$$U(0) \rightarrow \frac{U(0) \pm U(k_{1,+} - k_{1,-})}{2},$$

$$U(2k_F) \rightarrow \frac{U(2k_{1+}) \pm U(k_{1,+} + k_{1,-})}{2},$$

$$U(Q) \rightarrow \frac{U(k_{1,+} - k_{2,+}) \pm U(k_{1,+} - k_{2,-})}{2}, \qquad (18)$$

$$U(Q + 2k_F) \rightarrow \frac{U(k_{1,+} + k_{2,+}) \pm U(k_{1,+} + k_{2,-})}{2},$$

where the upper (lower) sign is for the symmetric (antisymmetric) solution.

For the symmetric solution, we have, formally keeping δ as an arbitrary number between $\delta = 0$ and $\delta = \pi/3$, at which the pockets disappear, and neglecting U_2,

$$\lambda_{s,\mathrm{I}}^{(1,s)} \approx -3U_0, \quad \lambda_{s,\mathrm{I}}^{(2,s)} = \lambda_{s,\mathrm{I}}^{(3,s)} = -U_1(\cos \delta + \cos 2\delta)^2,$$

$$\lambda_{t,\mathrm{I}}^{(1,s)} = 0, \quad \lambda_{t,\mathrm{I}}^{(2,s)} = \lambda_{t,\mathrm{I}}^{(3,s)} = 0, \qquad (19)$$

where $\mu = 4t\cos \delta(1 - \cos \delta)$. The symmetric solutions for Δ_i in various channels for the model I are shown in Fig. 11. For the f-wave solution, there are six zeros, one on each disconnected segment of the FS. For each d-wave solution, there are four nodes. For each p-wave solutions, there are two nodes. The signs of λ's in (19) are, however, such that at this level no superconductivity emerges down to $T = 0$ when U_0 and U_1 are positive.
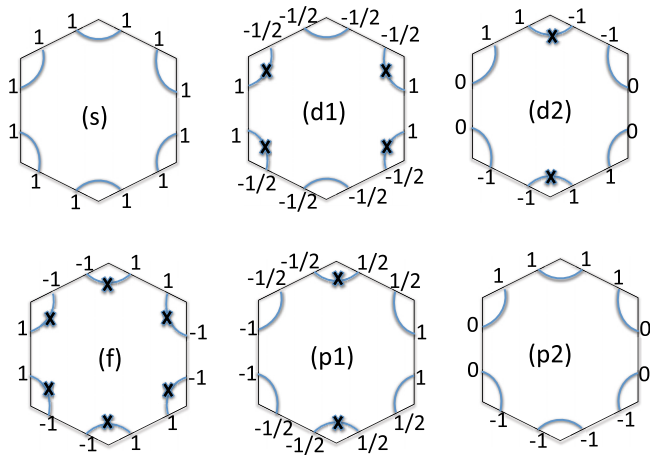
FIG. 11. (Color online) The structure of superconducting gaps in s-wave, f-wave, and two degenerate d-wave and p-wave channels for the symmetric solution for the patch model I for $\mu > 0$, when the FS consists of six disconnected pieces. About the same solutions are obtained in patch model II in s-wave and p-wave channels.

For the antisymmetric solution, we obtain, again neglecting U_2,

$$\lambda_{s,\text{I}}^{(1,a)} = 0, \quad \lambda_{s,\text{I}}^{(2,a)} = \lambda_{s,\text{I}}^{(3,a)} = 0,$$
$$\lambda_{t,\text{I}}^{(1,a)} = -4U_1 \sin^2 \delta (1 + \cos \delta)^2, \qquad (20)$$
$$\lambda_{t,\text{I}}^{(2,a)} = \lambda_{t,\text{I}}^{(3,a)} = -U_1 \sin^2 \delta (1 - 2\cos \delta)^2.$$

The structure of Δ_i in various channels is shown in Fig. 12. We keep calling the solutions s, p, d, and f waves, although the number of zeros on the FS now depends on whether the solution is symmetric or antisymmetric. In particular, the antisymmetric f-wave solution has no nodes on the FS (the nodes fall in between the Fermi pockets), while one of the antisymmetric d-wave solutions has nodes on each of six disconnected segments of the FS.
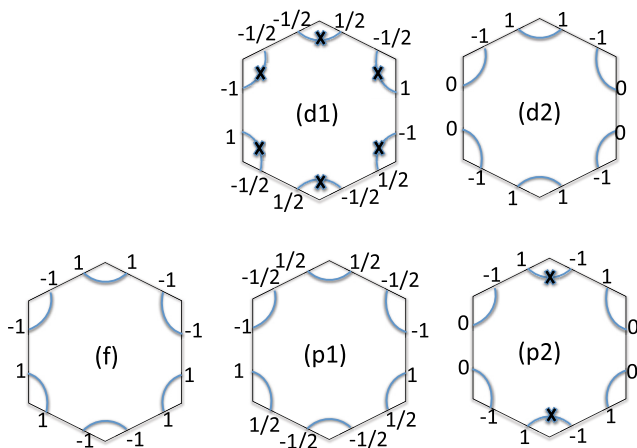

FIG. 12. (Color online) The same as in Fig. 11, but for the antisymmetric solution for the patch model I. About the same solutions are obtained in patch model II in f-wave and d-wave channels.
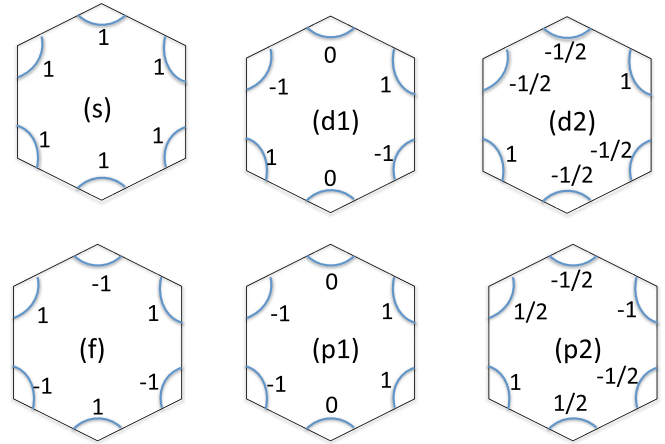

FIG. 13. (Color online) The structure of the gap in s-, p-, d-, and f-wave channels in patch model II at $0 < \mu < t$, when the FS consists of six disconnected segments.

Like for the symmetric case, the couplings in (20) are either repulsive or zero. In the formal limit $\delta = \pi/3$, when the FS segments shrink into points, we have negative $\lambda_{t,\text{I}}^{(1,a)} = -27U_1/4$ for the f-wave channel, however, the couplings in s-, p-, and d-wave channels all vanish.

For patch model II, we have

$$\lambda_{s,\text{II}}^{(1)} \approx -3U_0,$$
$$\lambda_{s,\text{II}}^{(2)} = \lambda_{s,\text{II}}^{(3)} = -\frac{U_1}{2}[2 + \cos 2\bar{\delta} - \cos \bar{\delta}(1 + 4\sin \bar{\delta}/2)],$$
$$\lambda_{t,\text{II}}^{(1)} = -4U_1 \cos^2 \bar{\delta}/2(1 + \sin \bar{\delta}/2)^2, \qquad (21)$$
$$\lambda_{t,\text{II}}^{(2)} = \lambda_{t,\text{II}}^{(3)} = -U_1 \cos^2 \bar{\delta}/2(1 - 2\sin \bar{\delta}/2)^2,$$

as in Eq. (17), but now $\mu > 0$ and $\bar{\delta} = 2\arcsin\left[(1 - \sqrt{(t-\mu)/t})/2\right]$ is positive. At $\bar{\delta} = \pi/3$, $\mu = t$ and FSs disappear.

We show the structure of eigenfunctions in various channels in Fig. 13. Comparing these solutions with those in patch model I and assuming that the system allows only symmetric or antisymmetric solutions with respect to the former position of van Hove points, we realize that the d-wave and f-wave eigenfunctions in patch model II (corresponding to $\lambda_{t,\text{II}}^{(1)}$ and $\lambda_{s,\text{II}}^{(2,3)}$) have the same structure as antisymmetric solutions in patch model I (the ones for $\lambda_{t,\text{I}}^{(1,a)}$ and $\lambda_{s,\text{I}}^{(2,a)} = \lambda_{s,\text{I}}^{(2,a)}$), while the eigenfunctions in s-wave and p-wave channels in patch model II (corresponding to $\lambda_{s,\text{II}}^{(1)}$ and $\lambda_{t,\text{II}}^{(2,3)}$) have the same structure as symmetric solutions in patch model I (the ones for $\lambda_{s,\text{I}}^{(1,s)}$ and $\lambda_{t,\text{I}}^{(2,s)} = \lambda_{t,\text{I}}^{(2,s)}$). The eigenvalues are again generally negative (repulsive), if U_0 and U_1 are positive, but vanish in d-wave and p-wave channels when $\bar{\delta} = \pi/3$, i.e., when the FS shrinks to points.

The conclusion of the analysis in this section is that there are multiple choices for the structure of the superconducting gap for fermions on a triangular lattice. The "basic" symmetry of the gap function is either s or p, or d, or f wave, but the structure of the gap in each representation depends on the choice of where the gap is maximized, what in our study implies the choice of the patch model. The eigenvalues in

various channels depend on the coordinate dependence of the screened Coulomb interaction $U(r)$. For repulsive interaction $U(r)$, which extends to second nearest neighbors, we found that the bare couplings in all pairing channels (i.e., the couplings to order U) are repulsive, but some are either zero or close to zero. The coupling in a conventional spin-singlet s-wave channel is repulsive and of order of the on-site interaction U_0. The couplings in other channels vanish in the Hubbard limit but are generally nonzero and repulsive in an extended Hubbard model which includes interaction between nearest and second nearest neighbors. In particular, in patch model I, the couplings in the spin-singlet channel are repulsive at the van Hove filing ($\mu = 0$), but the ones in the spin-triplet channel are strictly zero. At smaller fillings (negative μ), the bare couplings in all channels are repulsive. At larger fillings, when the FS is separated into six disconnected segments, the bare f-wave coupling is zero for the symmetric solution, and the bare d-wave coupling is zero for the antisymmetric solution. (Again, we remind that although translation by reciprocal lattice vectors can turn the six disconnected FS arcs into two connected nearly circular pieces, we have chosen to work with six disconnected arcs instead of two circles. The results are the same either way.) For this last solution, the coupling in p-wave channel gets smaller near full filling. In patch model II, the bare couplings are also repulsive at a generic filling, but the ones in d-wave and p-wave channels get smaller when the size of the FS shrinks.

D. Kohn-Luttinger renormalizations

We now extend this analysis to second order in U and include the renormalization of the pairing interaction by fermions with energies below the theory cutoff Λ. As noted in the introduction, such analysis has been first performed by Kohn and Luttinger (KL) for a 3D Fermi liquid with a generic short-range interaction, and second-order contributions to the pairing interactions are often called KL contributions. We will use this notation.

One can argue that KL renormalization is relevant at weak coupling only in a situation when the bare interaction is zero, otherwise there is a repulsion to first order in $U(q)$ and KL terms cannot overcome it. This is generally true if $U(q)$ is asymptotically small. However, we will see that attractive contributions to $\lambda_{s,1}^{(2,s)} = \lambda_{s,1}^{(3,s)}$ and $\lambda_{t,1}^{(1,a)}$ (symmetric d wave and antisymmetric f wave, respectively) appear at the second order in the on-site Hubbard interaction U_0. The first-order terms in these channels are repulsive, but are of order U_1. If, as it often happens, screened Coulomb interaction $U(r)$ rapidly drops with increasing r, we have $U_0 \gg U_1$. In this situation, the second-order contribution in U_0 becomes comparable to $O(U_1)$ already within weak coupling, when the perturbative approach is still valid (e,g., U_0^3 terms are small compared to KL terms).

In the rest of this section, we compute $O(U^2)$ terms near but still at some distance from van Hove filling. Right at van Hove filling, the KL U^2 terms contain logarithms that can only be cut by external temperature, and higher-order terms in U contain higher powers of divergent logarithms. In this situation, one cannot restrict the analysis to terms second order in U and has to sum up an infinite series of terms. We discuss van Hove

filling in more detail later in the paper, in Sec. IV. Here and in the next section, we assume that logarithms are cut by a nonzero $|\mu|$ and $U(q)$ is small enough such that perturbation theory is valid

The computation of the KL renormalization of the pairing interaction is straightforward and has been discussed several times in the literature (e.g., Ref. [32]). One has to dress the bare interaction by the renormalization in the particle-hole channel. Approximating $U(q)$ by U_0, one finds that only the exchange diagram in Fig. 1 contributes. In this situation, the renormalized interactions are

$$
\begin{aligned}
U_{\text{ren}}(k - k') &= U(k - k') + U_0^2 \Pi(k + k'), \\
U_{\text{ren}}(k + k') &= U(k + k') + U_0^2 \Pi(k - k'),
\end{aligned}
\tag{22}
$$

where $\Pi(q) = \int (d^2 l d\omega / (8\pi^3)) G(k,\omega) G(l + q,\omega)$ is the particle-hole polarization bubble (defined with a positive sign). For a circular FS in 2D, $\Pi(q < 2k_F) = m/(2\pi)$.

To understand what KL terms do, it is sufficient to consider the two limiting cases: (i) the case $\mu \approx t$, when disconnected FS segments are about to disappear, and (ii) a small deviation from van Hove point. To keep the presentation focused, we will not consider in detail how KL renormalization affects all possible channels, and instead will focus on the two most obvious choices—a spin-triplet nodeless f-wave state near $\mu \approx t$ and doubly degenerate d-wave state near $\mu = 0$. We show that for both states, KL terms are attractive, of order U_0^2, and well may overshoot repulsive terms of order U_1. We checked KL renormalization in other channels and found that they are not competitors to the two which we discuss below.

1. Near full filling

Near full filling, the most straightforward approach is to consider patch model II in which patches are centered in the middle of each FS segment. At $\mu \lesssim t$, one can easily make sure that there are only two relevant interactions $U_{\text{ren}}(0)$ and $U_{\text{ren}}(2k_F)$, as if we define the corner BZ points as $k_1 = (-\frac{4\pi}{3}, 0)$, $k_2 = (\frac{2\pi}{3}, \frac{3\pi}{\sqrt{3}})$, and $k_3 = (\frac{2\pi}{3}, \frac{3\pi}{\sqrt{3}})$, then $k_i - k_j$ is zero up to reciprocal lattice vector and $k_i + k_j = 2k_i$, again up to a reciprocal lattice vector. Then all we need to is to compute $\Pi(0)$ and $\Pi(2k_F)$.

The fermionic dispersion within each segment can be obtained by expanding near near the top of the band, i.e., for $k = (-\frac{4\pi}{3} + l_x, l_y)$, the dispersion

$$
\varepsilon(k) = (t - \mu) - \frac{3t}{4} l^2 - \frac{\sqrt{3}t}{8} l_x (l_x^2 - 3l_y^2) + \ldots . \tag{23}
$$

Evaluating the particle-hole bubbles $\Pi(0)$ and $\Pi(2k_F)$, we find that both the momentum integrals are dominated by small $\mathbf{l}$, where Eq. (23) is valid. The results are

$$
\begin{aligned}
\Pi(0) &\approx \frac{1}{\sqrt{3}} \frac{1}{\pi t}, \\
\Pi(2k_F) &= \frac{1}{2} \Pi(0) + \frac{\sqrt{3}}{54\pi t} \left(\frac{t - \mu}{t} \right) \approx \frac{1}{2} \Pi(0).
\end{aligned}
\tag{24}
$$

The approximate factor of 2 difference between $\Pi(0)$ and $\Pi(2k_F)$ can be easily understood. Indeed, $\Pi(0)$ is the sum of contributions from all six segments of the FS. Its independence on $t - \mu$ is the known result in 2D: after the frequency

integration in $\Pi(0) = \lim_{q\to 0} \int d^2 l\, d\omega G(l,\omega) G(l+q,\omega)$ the smallness of the phase space precisely cancels the smallness of the energy ε_l in the denominator. For $\Pi(2k_F)$, we find that $\varepsilon(l)$ and $\varepsilon(l+2k_F)$ are simultaneously small only in three FS segments out of six. In the other three, if we choose l to be on the FS, $\varepsilon(l_F + 2k_F)$ will be far from zero. For example, if we choose $2k_F = (-\frac{8\pi}{3},0)$, then $\varepsilon(l)$ and $\varepsilon(l+2k_F)$ are both small for l near $(\frac{4\pi}{3},0)$, $(-\frac{2\pi}{3},\frac{2\pi}{\sqrt{3}})$, and $(-\frac{2\pi}{3},-\frac{2\pi}{\sqrt{3}})$, while for l near $(-\frac{4\pi}{3},0)$, $(\frac{2\pi}{3},\frac{2\pi}{\sqrt{3}})$, and $(\frac{2\pi}{3},-\frac{2\pi}{\sqrt{3}})$, ε_l is small, but $\varepsilon(k+2k_F) \approx -9t$. The contribution from these three corners is then small in $t-\mu$ [the second term in $\Pi(2k_F)$ in (24)].

Using $\Pi(2k_F) \approx (1/2)\Pi(0)$, we obtain, keeping only terms in U_0,

$$U_{\text{ren}}(0) = U_0 + \frac{1}{2}U_0^2\Pi(0),$$

$$U_{\text{ren}}(2k_F) = U_0 + U_0^2\Pi(0), \qquad (25)$$

$$\Pi_0 = \frac{1}{\sqrt{3}\pi t}.$$

Substituting these U_{ren} into the spin-singlet and spin-triplet components of the vertex function and re-evaluating λ_i in different channels, we find that the KL term gives a positive (attractive) contribution of order $U_0^2\Pi(0)$ to f-wave coupling:

$$\lambda_f = \lambda_{t,\text{II}}^{(1)} + \frac{3}{4}U_0^2\Pi(0) \approx -\frac{27}{4}U_1 + \frac{\sqrt{3}}{4\pi}\frac{U_0^2}{t}. \qquad (26)$$

We see that the interaction in the f-wave channel in the patch model II (same as in the antisymmetric f-wave channel in patch model I) becomes attractive if the second-order KL contribution from the on-site interaction U_0 exceeds the repulsive first-order contribution from the nearest-neighbor interaction U_1. We remind the reader that the antisymmetric f-wave solution is the one in which the gap does not change sign along a given FS segment but changes sign between nearest FS segments.

Suppose that the KL contribution is larger than the bare repulsion and the interaction in f-wave channel is attractive. We then have $T_{c,f} \sim \varepsilon_F e^{-1/\bar{\lambda}_f}$, where $\varepsilon_F \sim t-\mu$, and $\bar{\lambda} = \lambda_f/(3\sqrt{3}\pi t)$ is the dimensionless coupling. We have, without the U_1 term, $\bar{\lambda}_f = (1/12\pi^2)(U_0/t)^2 \approx 0.68(U_0/W)^2$, where $W = 9t$ is the bandwidth. Note that T_c vanishes at $\mu = t$ due to the vanishing prefactor. However, the coupling $\bar{\lambda}_f$ remains finite in this limit. This last result is a peculiarity of 2D where the density of states on the FS does not depend on the value of Fermi momentum.

One can easily extend the analysis to order $O(t-\mu)$ and analyze how $T_{c,f}$ evolves with decreasing μ. We found that the f-wave coupling *increases* with increasing fermionic density. Explicitly,

$$\bar{\lambda}_f = \frac{1}{12\pi^2}\left(\frac{U_0}{t}\right)^2\left(1 + \frac{5}{9}\frac{t-\mu}{t}\right). \qquad (27)$$

As a result, f-wave pairing gets stronger as one moves away from full to van Hove filling [see Fig. 14(a)].

For completeness and for comparison of the couplings between f-wave and d-wave channels later in the paper, we computed the KL renormalization of the coupling $\lambda_{s,\text{I}}^{(2,s)}$ for the
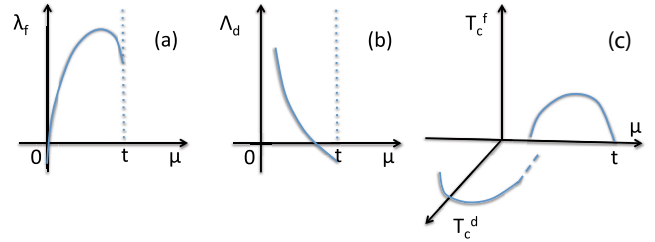

FIG. 14. (Color online) (a) and (b) The coupling constants in f-wave and in d-wave channels as functions of the chemical potential for fermions on a triangular lattice. (c) The transition temperatures for f-wave and chiral $d+id$ superconductivity. The coupling in f-wave channel remains finite and positive at $\mu = t$, when the FS disappears, but T_c for f-wave vanishes because of vanishing prefactor. Near van Hove doping, f-wave channel is already repulsive. As a result, T_c for f wave is peaked in between $\mu = 0$ and $\mu = t$. The degenerate d-wave channel has the largest coupling at van Hove doping, but becomes repulsive at $\mu \approx t$. Whether the attractive regions in d-wave and f-wave channels overlap depends on the interplay between KL terms and the first-order terms coming from interaction between first, second, and, possibly, further neighbors. Moreover, at intermediate μ, SDW well may become the leading instability.

symmetric d-wave channel in patch model I. We found that for this coupling, which we relabel as λ_d for clarity, KL terms make the initially repulsive interaction even more repulsive. Specifically,

$$\lambda_d = \lambda_{s,\text{I}}^{(2,s)} - \frac{3}{4}U_0^2\Pi(0) \approx -\frac{\sqrt{3}}{4\pi}\frac{U_0^2}{t} < 0. \qquad (28)$$

2. Near van Hove filling

Continue first with the coupling in the f channel in patch model II. Near van Hove doping, the expression for λ_f is

$$\lambda_f = \lambda_{t,\text{II}}^{(1)} + \frac{U_0^2}{2}[\Pi(0) + 2\Pi(Q) \\ - \Pi(2k_F) - 2\Pi(Q + 2k_F)]. \qquad (29)$$

For $\mu \approx 0$, all four Π's are different and have contributions from low-energy fermions from different numbers of patches. $\Pi(0)$ is the sum of contributions from low-energy fermions in all six patches. For $\Pi(Q)$ and $\Pi(Q + 2k_F)$, such contributions come from two patches, and for $\Pi(2k_F)$ the low-energy contribution comes from only one patch. Away from the immediate vicinity of van Hove filling, all individual low-energy contributions are roughly of the same order. Then the $\Pi(0)$ term is the largest (because of the largest number of contributions), i.e., the U_0^2 term in λ_f is attractive and can easily exceed a small repulsive bare term $\lambda_{t,\text{II}}^{(1)} \approx -4U_1$ [see Eq. (17)]. As a consequence, the f-wave channel remains attractive. However, right at van Hove filling this is no longer the case because $\Pi(2k_F)$ diverges logarithmically, as $\ln \Lambda/T$, and overshoots $\Pi(0)$. The terms $\Pi(Q)$ and $\Pi(Q + 2k_F)$ diverge even more strongly, as $\ln^2(\Lambda/T)$, but the two are identical at $\mu = 0$ and cancel out in Eq. (29). As a result, the U_0^2 contribution to f-wave coupling in (29) is negative at $\mu = 0$, i.e., the coupling in the f-wave channel becomes repulsive near van Hove filling. In Fig. 14, we combine the results for

λ_f near van Hove and near full filling and sketch the behavior of λ_f at fermionic densities between the two limits. We clearly see that λ_f is nonmonotonic and has a maximum somewhere between van Hove and full filling. The nonmonotonic behavior of the coupling combined with the $t - \mu$ dependence of the prefactor for T_c gives rise to a nonmonotonic behavior of the onset temperature for f-wave pairing, as shown in Fig. 14.

We next analyzed patch model I, in which the gap is concentrated near van Hove points. We found that the most relevant KL contribution near van Hove filling is in the doubly degenerate (symmetric) d-wave channel. The coupling in this channel is

$$\lambda_d = \lambda_{s,\mathrm{I}}^{(2,s)} + \frac{U_0^2}{2}[-\Pi(0) - \Pi(2k_F) + \Pi(Q) + \Pi(Q + 2k_F)], \tag{30}$$

and at small μ, $\lambda_{s,\mathrm{I}}^{(2,s)} \approx -U_1$. The terms $\Pi(Q)$ and $\Pi(Q + 2k_F)$ are identical at $\mu = 0$ and both diverge as $\log^2 \Lambda/T$, hence at small T the U_0^2 term definitely exceeds the bare repulsion. Then $\lambda_d > 0$, i.e., the d-wave channel is attractive.

As has already been mentioned the presence of the logarithms in the perturbation theory implies that one cannot restrict oneself to the lowest order in perturbation theory and has to sum an infinite series of KL-type corrections to the pairing interaction. We discuss this in detail in Sec. IV. The conclusion is qualitatively the same as the one obtained from the lowest order calculation. Namely, the two d-wave components are degenerate and attractive near van Hove filling, and the corresponding T_c has a maximum value right at van Hove filling (see, e.g., Refs. [25,27,32]. The superposition of the two degenerate states can be chosen such that they are related by time reversal. Below T_c, the system spontaneously chooses one of the states in order to maximize condensation energy and, by doing so, breaks time-reversal symmetry.

We combine the results for λ_d at small μ and at $\mu \approx t$ and sketch the behavior of d-wave coupling between van Hove and full filling in Fig. 14(b). The comparison between this figure and Fig. 14(a) shows that the system undergoes a transition from d-wave to f-wave pairing at some distance from van Hove doping [Fig. 14(c)]. At a truly weak coupling, T_c is the largest right at van Hove filling.

Like we said, we analyzed other channels, i.e., symmetric and antisymmetric p, symmetric f, and antisymmetric d waves, and found that they are not competitors to symmetric d and antisymmetric f channels. We also analyzed the pairing at smaller fillings, when $\mu < 0$. We found that the f-wave channel again is the most attractive, because $\Pi(0)$ is the largest. Hence, as filling decreases from the full one, the largest attractive coupling evolves from f to d wave, and then again to f wave. This agrees with the numerical study in Refs. [20,33]. We note that the f-wave gap for $\mu < 0$, where the FS consists of one piece, changes sign six times as one moves along the FS.

III. FERMIONS ON A HONEYCOMB LATTICE

A similar but not identical behavior emerges in the KL analysis of an interacting system of fermions on a honeycomb lattice. This is what we analyze next.
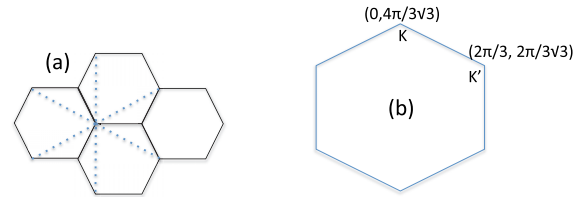

FIG. 15. (Color online) A honeycomb lattice (a) and the corresponding Brillouin zone in momentum space (b).

A. FS and fermionic dispersion

A honeycomb lattice is presented in Fig. 15. There are two nonequivalent lattice sides, marked K and K' in the figure. In a tight-binging model, fermions hop from one sublattice to the other. The corresponding Hamiltonian in momentum space is [34]

$$\mathcal{H}_2 = -\sum_k [\gamma_k a_k^\dagger b_k + \gamma_k^* b_k^\dagger a_k - \mu(a_k^\dagger a_k + b_k^\dagger b_k)], \tag{31}$$

where

$$\gamma_k = t\left(e^{-ik_x} + 2e^{ik_x/2}\cos\frac{k_y\sqrt{3}}{2}\right). \tag{32}$$

It is convenient to define $\gamma_k = \varepsilon_k e^{i\phi_k}$, where

$$\varepsilon_k = |\gamma_k| = t\sqrt{1 + 4\cos\frac{3k_x}{2}\cos\frac{k_y\sqrt{3}}{2} + 4\cos^2\frac{k_y\sqrt{3}}{2}} \tag{33}$$

and

$$\cos\phi_k = \frac{\cos k_x + 2\cos\frac{k_x}{2}\cos\frac{k_y\sqrt{3}}{2}}{\varepsilon_k}, \quad \phi_{-k} = -\phi_k. \tag{34}$$

The quadratic form is diagonalized by unitary transformation

$$\begin{aligned} a_k &= \frac{1}{\sqrt{2}}e^{i\phi_k/2}(c_k + d_k), \\ b_k &= \frac{1}{\sqrt{2}}e^{-i\phi_k/2}(c_k - d_k). \end{aligned} \tag{35}$$

The excitation spectrum consists of two branches with opposite signs of energy

$$\mathcal{H}_2 = \sum_k [(\varepsilon_k - \mu)d_k^\dagger d_k - (\varepsilon_k + \mu)c_k^\dagger c_k]. \tag{36}$$

At half-filling, $\mu = 0$, the FS consists of 6 Dirac points $(\pm 2\pi/3, \pm 2\pi/(3\sqrt{3})), (0, \pm 4\pi/(3\sqrt{3}))$ at which $\varepsilon_k = 0$. Only two of these six Dirac points are inequivalent (the rest are connected by reciprocal lattice vectors), but it is convenient for our analysis to work keep track of excitations near all six Dirac points. The same results are (of course) obtained if we identify points that differ by a reciprocal lattice vector. When filling either increases or decreases, 6 disconnected segments of the FS open up. At 3/8 or 5/8 filling, when $|\mu| = t$, disconnected FS pieces merge. At these two fillings, the excitation spectrum has six van Hove points at $(\pm 2\pi/3, 0)$ and $(\pm \pi/3, \pm \pi/\sqrt{3})$ and the FS obtained from (33) consists of straight lines connecting van Hove points. The van Hove

points are protected by topology and survive when hopping extends beyond nearest neighbors. The nesting (FS in the form of straight lines) survives when the hopping extends to second neighbors, but gets destroyed by third and further neighbor hoppings. At larger $|\mu|$, the FS has one piece, centered in the middle of the BZ. The size of the FS shrinks and it vanishes at $|\mu| = 3t$. This evolution is quite similar to the one in Fig. 5 for the triangular lattice.

For positive μ (filling above $1/2$), the six disconnected FSs are of electron type (the states inside the FS have smaller energy than μ) and the FS centered at $(0,0)$ is of hole type. For negative μ, the situation is opposite. The cases of positive and negative μ give identical results for superconductivity, and for definiteness below we focus on $\mu > 0$ when d_k fermions have a FS [see Eq. (36)].

B. The pairing interaction

We use the same general reasoning as in the previous paragraph. Namely, we split the antisymmetrized interaction into spin-singlet and spin-triplet components and further split spin-singlet component into s wave ($\lambda_s^{(1)}$) and doubly degenerate d wave ($\lambda_s^{(2)} = \lambda_s^{(3)}$) and split spin-triplet component into f wave ($\lambda_t^{(1)}$) and doubly degenerate p wave ($\lambda_t^{(2)} = \lambda_t^{(3)}$). To shorten the presentation and not to bother the reader with a rederivation of the same results as in the previous section, we only consider the range of doping where the FS consists of six disconnected segments. We consider patch model I, in which the pairing predominantly involves fermions from momenta near where van Hove points are located at van Hove doping. Like in the triangular case, we consider two types of the solutions for the gap: the "symmetric" solution, in which the gap remains of the same sign at the two ends when we split each van Hove point into two, and the "antisymmetric" one, in which the gap changes sign between the two split van Hove points. In another parallel to the triangular case, we also consider patch model II, in which we focus on the middle points of the disconnected FS segments. We again find that the solutions for the gap in the patch model II are similar to the solutions of the antisymmetric model I in d-wave and f-wave channels and to the solutions of the symmetric model I in p-wave and s-wave channels.

The structure of the gap in various channels in these two patch models is quite similar to that on the triangular lattice (see Figs. 11–13), the only difference is that the FS for the honeycomb lattice is rotated by $90°$ compared to that for the triangular lattice. For this reason, we will not present separate figures for the gap structures on a honeycomb lattice.

C. First order in $U(q)$

Like in the triangular lattice case, we consider the lattice model with short-range interaction, which extends up to second neighbors. The interaction is originally written in real space in terms of lattice operators a and b. To re-express it in terms of operators d_k and $d_k^\dagger$ one needs to apply the unitary transformation, i.e., include the phase factors. These phase factors are often neglected in the literature. We will see, however, that they play an important role in our case.

1. Extended Hubbard model

We consider the model with interaction up to second neighbors. The on-site interaction potential involves fermions from the same sublattice and phase factors cancel out for incoming momenta $k, -k$ and outgoing momenta $p, -p$:

$$H_{\text{int}}^{(0)} = -\frac{U_0}{2}(a_{k,\alpha}^\dagger a_{-k,\beta}^\dagger a_{p,\alpha} a_{-p,\beta} + b_{k,\alpha}^\dagger b_{-k,\beta}^\dagger b_{p,\alpha} b_{-p,\beta})$$
$$= -\frac{U_0}{4} d_{k,\alpha}^\dagger d_{-k,\beta}^\dagger d_{p,\alpha} d_{-p,\beta}. \tag{37}$$

Interaction between nearest neighbors involves fermions from different sublattices, and phase factors do not cancel and have to be kept [18]. We obtain

$$H_{\text{int}}^{(1)} = -\frac{U_1}{8} d_{k,\alpha}^\dagger d_{-k,\beta}^\dagger d_{p,\alpha} d_{-p,\beta} \varepsilon_{k-p} \cos(\phi_{k-p} - \phi_k + \phi_p). \tag{38}$$

Interaction between second neighbors again involves fermions from the same sublattice and phase factors cancel out:

$$H_{\text{int}}^{(2)} = -\frac{U_2}{2} d_{k,\alpha}^\dagger d_{-k,\beta}^\dagger d_{p,\alpha} d_{-p,\beta} \Phi(k - p),$$
$$\Phi(q) = \cos q_y \sqrt{3} + 2 \cos \frac{3q_x}{2} \cos \frac{q_y \sqrt{3}}{2}. \tag{39}$$

Like before, we assume $U_0 \gg U_1 \gg U_2$ and will only keep the leading term in the formulas for the eigenvectors.

a. Van Hove filling, $\mu = t$. Consider first the patch model I, which is centered at van Hove points. For a given triad $k_1 = (-2\pi/3, 0)$, $k_2 = (\pi/3, \pi/\sqrt{3})$, and $k_3 = (\pi/3, -\pi/\sqrt{3})$ we have $\phi_{k_i} = -\pi/3$ ($i = 1, 2, 3$) and $\phi_{k_i - k_j} = \pi$ for $i \neq j$. Like in triangular case, there are only two different interactions $U(0) = U(2k_F)$ and $U(Q) = U(Q + 2k_F)$, where $Q = k_1 - k_2$. A simple calculation yields

$$U(0) = \frac{U_0}{2} + \frac{3U_1}{4} + \frac{3U_2}{2},$$
$$U(Q) = \frac{U_0}{2} - \frac{U_1}{4} - \frac{U_2}{2}. \tag{40}$$

The interaction in the spin-triplet channel then vanishes identically, and in spin-singlet channel, we obtain

$$\lambda_s^{(1)} \approx -3\frac{U_0}{2} - U_1 - U_2, \quad \lambda_s^{(2)} = \lambda_s^{(3)} = -U_1 - U_2. \tag{41}$$

Both couplings are repulsive if U_i are all positive.

The patch model II at van Hove filling is centered at $\pm \bar{k}_1$, $\pm \bar{k}_1$, and $\pm \bar{k}_1$, where $\bar{k}_1 = (0, \pi/\sqrt{3})$, $\bar{k}_2 = (-\pi/2, -\pi/(2\sqrt{3}))$, and $\bar{k}_3 = (\pi/2, -\pi/(2\sqrt{3}))$. For this model, the eigenvalues are nonzero in all channels. We obtained

$$\lambda_{s,\text{II}}^{(1)} = -3\frac{U_0}{2}, \quad \lambda_{s,\text{II}}^{(2)} = \lambda_{s,\text{II}}^{(3)} = -\frac{U_1}{4},$$
$$\lambda_{t,\text{II}}^{(1)} = -2U_2, \quad \lambda_{t,\text{II}}^{(2)} = \lambda_{t,\text{II}}^{(3)} = -\frac{3U_1}{4}. \tag{42}$$

Again, all eigenvalues are negative (repulsive), when all $U_i > 0$.

b. Larger filling, $\mu > t$. The analysis parallels the one for fermions on a triangular lattice and we just list the results. The patch model I is centered at $(\pm \frac{2(\pi-\delta)}{3}, 0)$ and $(\pm \frac{(\pi-\delta)}{3}, \pm \frac{(\pi-\delta)}{\sqrt{3}})$,

where δ is related to μ as $\mu = t\sqrt{1 + 8\sin^2\delta/2}$. The center for each patch is the saddle point in the fermionic dispersion, e.g., near $k_1 = (-\frac{2(\pi-\delta)}{3}, 0)$,

$$\varepsilon_{k_1+k} = -3(\sin\delta/\sqrt{1 + 8\sin^2\delta/2})k_x,$$
$$- (3/2)((1 - 0.5\cos\delta)/\sqrt{1 + 8\sin^2\delta/2})k_y^2. \quad (43)$$

The eigenvalues are

$$\lambda_s^{(1)} = -3\frac{U_0}{2}, \quad \lambda_s^{(2)} = \lambda_s^{(3)} = -\frac{U_1}{4}\frac{(1 + \cos\delta)^2}{5 - 4\cos\delta},$$
$$\lambda_t^{(1)} = 0, \quad \lambda_t^{(2)} = \lambda_t^{(3)} = -\frac{9U_1}{4}\frac{\sin^2\delta}{5 - 4\cos\delta}. \quad (44)$$

Observe that the coupling in the f-wave channel vanishes, i.e., individual contributions from U_0, U_1, and U_2 all cancel out.

The patch model II is centered at $(0, \pm\frac{(\pi+\delta)}{\sqrt{3}})$ and $(\pm\frac{(\pi+\delta)}{2}, \pm\frac{(\pi+\delta)}{2\sqrt{3}})$, where $\bar{\delta} = -2\arcsin(\mu - t)/2$. The eigenvalues are

$$\lambda_{s,\text{II}}^{(1)} = -3\frac{U_0}{2}, \quad \lambda_{s,\text{II}}^{(2)} = \lambda_{s,\text{II}}^{(3)} = -\frac{U_1}{4}(1 + \sin\bar{\delta}/2)^2,$$
$$\lambda_{t,\text{II}}^{(1)} = -2U_2\cos^2\bar{\delta}/2(1 + \sin\bar{\delta}/2)^2, \quad (45)$$
$$\lambda_{t,\text{II}}^{(2)} = \lambda_{t,\text{II}}^{(3)} = -\frac{2U_1}{8}(1 + \cos\bar{\delta}).$$

All bare couplings are again repulsive. Note, however, that the coupling in the f-wave channel is proportional to the second-neighbor interaction potential U_2, i.e., it is smaller than the repulsive couplings in other channels.

c. Smaller fillings $0 < \mu < t$. In this range of fillings, the FS consists of 6 segments around Dirac points. For the patch model II, the eigenfunctions are the same as in Eq. (45), only now $\bar{\delta}$ is positive and varies between $\bar{\delta} = 0$ at $\mu = t$ and $\bar{\delta} = \pi/3$ at $\mu = 0$. The couplings are all repulsive, the smallest is in the f channel, and this one varies between $\lambda_{t,\text{II}}^{(1)} = -2U_2$ at $\mu = 0$ and $\lambda_{t,\text{II}}^{(1)} = -27U_2/8$ at $\mu = t$.

Like in the triangular lattice case, the solutions for the gap for patch model I split into symmetric and antisymmetric subclasses, which differ in the relative signs of the gaps at split van Hove points (k_{i+} and k_{i-}). The formulas for the couplings are rather complicated due to the presence of phase factors in the nearest-neighbor interaction and we do not present them here. The key result is that the couplings are repulsive in all channels except in symmetric spin-triplet channels and antisymmetric spin-singlet channels, where individual contributions of order U_1 and U_2 cancel out for all $0 < \mu < t$. In technical terms, the cancellation holds between $U(0)$ and $U(k_{1+} + k_{1-})$, between $U(k_{1+} - k_{2+})$ and $U(k_{1+} + k_{2,-})$, etc.

To summarize, we see that the couplings to order $U(q)$ are generally repulsive, although the one for the f-wave channel in the model II (similar to the one in the antisymmetric f-wave channel in model I) is only repulsive due to second-neighbor $U_2 > 0$. As a peculiarity of the honeycomb lattice, the coupling in the symmetric spin-triplet f-wave channel vanishes for all dopings, and the couplings in the symmetric p-wave channel and antisymmetric s and d channels vanish for all $0 < \mu < t$. The antisymmetric solution in the patch model I indeed only makes sense when the FS consists of separate segments.

D. Kohn-Luttinger renormalizations

We now discuss the KL physics: the renormalization of the interactions to second order in U. Like in the triangular case, we search for the renormalizations coming from on-site interaction as attraction and hope that a KL attraction at order U_0^2 can overshoot a bare repulsion of order U_1 or, even better, U_2. We again consider the two limiting cases: one close to half-filling, when FS segments around Dirac points are small, and the other near van Hove filling.

1. Near half-filling

We first consider patch model I and look into the channels for which the couplings to order $O(U_0)$ vanish. These are antisymmetric spin singlet and symmetric spin-triplet channels. If there was an attraction in any of these channels from KL terms, the system would become a superconductor for arbitrarily weak interaction $U(q)$. We found, however, that this does not happen. Namely, the KL renormalizations in these particular channels involve the combinations of polarization operators:

$$\Pi(0) - \Pi(k_{1+} + k_{1-}), \Pi(k_{1+} - k_{1-}) - \Pi(2k_{1+}),$$
$$\Pi(k_{1+} - k_{2+}) - \Pi(k_{1+} + k_{2-}), \Pi(k_{1+} - k_{2-})$$
$$- \Pi(k_{1+} + k_{2+}). \quad (46)$$

A straightforward analysis shows that these combinations are all zero. For example, for $k_{1+} = (2\pi/3, \delta/\sqrt{3})$, $k_{1-} = (2\pi/3, -\delta/\sqrt{3})$, where $\delta = 2\arccos(t - \mu)/2t$, $\varepsilon_{k_{1+}+k_{1-}+q} = \varepsilon_q$. and $\varepsilon_{k_{1-}-k_{1-}+q} = \varepsilon_{2k_{1+}+q}$. Elementary analysis then shows up that each of the terms in Eq. (46) vanishes. The implication is that, in patch model I, the pairing interaction in these particular channels vanishes to order U_0^2 and, we conjecture, to all orders in U_0. This vanishing is the consequence of FS nesting, which is present as long as one neglects third neighbor and longer range hopping. Hopping between third neighbors breaks nesting and gives rise to nonzero couplings in the antisymmetric spin singlet and symmetric spin-triplet channels. The third neighbor hopping is, however, rather weak, at least in graphene, and these pairing interactions, even if attractive, are weak compared to interactions in the antisymmetric f-wave and symmetric d-wave channels, which we consider below.

Antisymmetric f-wave and symmetric d-wave channels can be conveniently studied at small μ within patch model II, and we now focus on this model. Like in the case of a triangular lattice, there are two relevant interactions $U_{\text{ren}}(0)$ and $U_{\text{ren}}(2k_F)$. Keeping only the U_0 term we obtain, like before,

$$U_{\text{ren}}(0) = \frac{U_0}{2} + \frac{1}{4}U_0^2\Pi(2k_F),$$
$$U_{\text{ren}}(2k_F) = \frac{U_0}{2} + \frac{1}{4}U_0^2\Pi(0),$$
$$U_{\text{ren}}(Q) = \frac{U_0}{2} + \frac{1}{4}U_0^2\Pi(2k_F), \quad (47)$$
$$U_{\text{ren}}(Q + 2k_F) = \frac{U_0}{2} + \frac{1}{4}U_0^2\Pi(0),$$

where Q is approximately the distance between Dirac points. Again, the polarization operator $\Pi(0)$ at zero momentum

transfer is approximately two times larger than the one at $2k_F$ because $\Pi(0)$ collects the contributions from low-energy fermions from all six segments of the FS, while $\Pi(2k_F)$ collects low-energy contributions from three segments, and in other three the momentum transfer by $2k_F$ places a fermion far away from the FS. As a result, the coupling in the f-wave channel is

$$\lambda_f = \lambda_{t,II}^{(1)} + \frac{3}{8}U_0^2 \left[\Pi(0) - \Pi(2k_F)\right]$$

$$\approx -27\frac{U_2}{8} + \frac{3}{16}U_0^2\Pi(0). \quad (48)$$

We see that, like in the triangular case, the U_0^2 term in the interaction is attractive [$\Pi(0)$ is positively defined]. Because $U_0 \gg U_2$, the KL term overshoots the bare repulsion already at weak coupling. Once this happens, the system becomes unstable against f-wave pairing of the same type as Fig. 13.

There is one difference with the triangular case though. The evaluation of $\Pi(0)$ yields [35]

$$\Pi(0) = \frac{2\mu}{\sqrt{3}\pi t^2} + O(\mu^2). \quad (49)$$

In distinction to the case of a triangular lattice, the polarization operator $\Pi(0)$ scales linearly with μ and vanishes right at half-filling. This implies that f-wave attraction develops only at some small but finite distance away from from half-filling, when the KL attractions develops enough to overshoot the first-order repulsion. An additional smallness at $\mu \ll t$ comes from the fact that the actual parameter that appears in the exponent in the BCS formula for T_c is the product of $\lambda_{t,II}^{(1,\mathrm{ren})}$ and the density of states at the FS. The latter also scales with μ:

$$N_F = \frac{\mu}{3\pi t^2} + O(\mu^2). \quad (50)$$

Introducing the dimensionless coupling $\bar{\lambda} = \lambda N_F$, we obtain for the f-wave channel

$$\bar{\lambda}_f = -\frac{9}{8\pi}\left(\frac{U_2}{t}\right)^2\left(\frac{\mu}{t}\right) + \frac{\sqrt{3}}{24\pi^2}\left(\frac{U_0}{t}\right)^2\left(\frac{\mu}{t}\right)^2. \quad (51)$$

Superconducting $T_c \sim \mu e^{-1/\bar{\lambda}_f}$. At small μ/t, T_c is vanishingly small, if not zero. However, at, say, $U_0 \sim 6t$ (the bandwidth) and $\mu \lesssim t$ the dimensionless coupling is $\bar{\lambda}_f \approx 0.26$ and $T_c \sim 10^{-3}t$, which is not small given that $t \sim 10^4$ K.

There is an interesting peculiarity of f-wave pairing on a honeycomb lattice: the gap has a nonvanishing angular dependence at small μ. This follows from the fact that if one calculates $\Pi(q)$ for Dirac fermions at small μ without approximating $\Pi(q)$ by $\Pi(0)$, we obtain a universal dependence on q/k_F:

$$\Pi(q) = \frac{2\mu}{\pi\sqrt{3}t^2}f\left(\frac{q}{k_F}\right), \quad (52)$$

where $k_F = 2\mu/(3t)$. In the two limits, $f(0) = 1$ and $f(2) = 3.66/\pi$. In between, $f(x)$ interpolates as shown in Fig. 16. Because of this dependence, if we label by ϕ and ϕ' the angles specifying the locations of fermions on the FS's ($-\pi/3 < \phi, \phi' < \pi/3$), the kernel in the gap equation relating $\Delta(\phi)$ and $\Delta(\phi')$ contains the function of $\cos(\phi - \phi')$. A symmetric in ϕ solution is then $\Delta(\phi) = \Delta(1 + \alpha\cos\phi + $
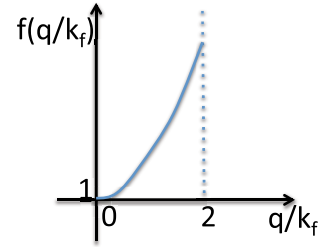

FIG. 16. (Color online) Scaling function $f(q/k_F)$ in Eq. (52). The limiting values are $f(0) = 1$ and $f(2) = 3.66/\pi$.

$\beta\cos^2\phi + \dots$), where α, β, etc., are universal numbers independent on μ.

We close this section with a word of caution. At second order in U, the presence of the other branch of excitations [c branch at negative energies in Eq. (36)] does not affect KL consideration for two reasons. First, the interactions in d-c basis do not contain terms with three d operators and one c operator, hence there are no KL contribution with the bubbles made out of one d and one c fermion. Second, the terms with two c and two d fermions are present, but these contain a polarization bubble made of two c fermions. The latter vanishes because the bubble is identically zero for any positive μ. However, at higher orders, diagrams of the type shown in Fig. 17 do contribute. These diagrams contain pairs of polarization bubbles, each made out of one c and one d fermion. Such a bubble tends to a finite value at vanishing μ, hence the dimensionless coupling from such term contains only one power of μ (but higher power of U/t). Whether these terms are friends or foes of f-wave superconductivity is unclear.

2. Near van Hove points

The consideration near van Hove points is essentially identical to the one for fermions on a triangular lattice and we only state the result: to order U_0^2 interaction in symmetric d-wave channel in patch model I is attractive and is logarithmically singular. The coupling in f-wave channel in patch model II) is repulsive at this density. The behavior of λ_d and λ_f at various densities is shown in Fig. 18 together with the corresponding T_c.

As a consequence, within the KL approximation, the strongest pairing instability at and near the van Hove points is doubly degenerate d wave. Whether there is a direct transition between f wave at smaller μ and d wave at $\mu \approx t$ (and possible co-existence of the two superconducting orders), or the system
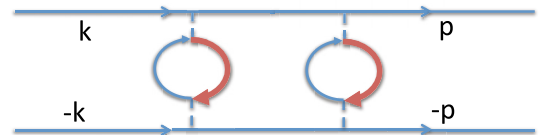

FIG. 17. (Color online) An example of higher-order diagram, which contributes to KL renormalization of the pairing interaction near half-filling. Thin blue and thick red lines represent fermions from the two branches with positive and negative energies, respectively. The dashed line is the Hubbard interaction $U(0)$.
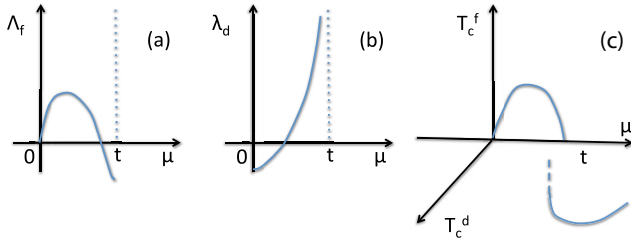
FIG. 18. (Color online) Fermions on a honeycomb lattice. (a) and (b) Behavior of the leading eigenfunctions in f-wave and d-wave channels as functions of the chemical potential for $0 < \mu < t$, when the FS consists of six disconnected segments. (c) Behavior of T_c in the two channels. The d-wave channel has the strongest instability (largest T_c) near van Hove doping.

first loses d-wave order, remains normal down to $T = 0$ in some range of $\mu \leqslant t$ and then becomes unstable towards f-wave superconductivity, depends on details. An SDW order at intermediate μ is also a possibility [18,27–29]. Numerical study of the Hubbard model with only U_0 interaction indicates that superconductivity of one type or the other develops for all $\mu < t$. How the situation changes due to interaction between further neighbors remains to be seen.

At even larger $\mu > t$, the analysis of superconductivity becomes less universal because the polarization operators $\Pi(0)$, $\Pi(2k_F)$, $\Pi(Q)$, and $\Pi(Q + 2k_F)$ are all of the same order and the interplay between them depends on the details of the band structure. If $\Pi(q)$ drops rather fast with increasing q, the f-wave channel again becomes attractive and wins over other channels. If so, the system evolves from f to d wave and then again to f-wave superconductor as μ increases. However, the coupling gets smaller as μ increases, so the best chance to detect f-wave superconductivity is to analyze the region $\mu \leqslant t$.

In the rest of the paper, we present more detailed analysis of superconductivity and its interplay with other instabilities near van Hove filling. Like we said, at van Hove doping the polarization operators at all four relevant momenta diverge logarithmically, either as $\ln \Lambda / T$ or as $\ln^2 \Lambda / T$, and the second-order KL analysis is not adequate.

IV. AT THE VAN HOVE POINT

When fermions on triangular or honeycomb lattices with hopping between nearest neighbors are doped to the saddle points of the dispersion, they display a nested FS (FS) and a logarithmically divergent density of states (DOS), which trigger instabilities to numerous strongly ordered states. It has recently been shown using a RG calculation that the leading instability in the presence of weak repulsive interactions is to chiral d wave superconductivity. However, that calculation only took into account the "corners" of the FS, which are saddle points of the dispersion and dominate the DOS. Here, we present the RG for the full FS.

We divide the FS up into corner regions (which are close to a saddle point and dominate the DOS) and "edge" regions. Ignoring the edges altogether corresponds to the RG from Ref. [25]. Here, we will take the edge regions into account

also. Initially, we work within a leading log approximation (valid in the weak coupling limit), and demonstrate that the behavior of the FS edges mimics the behavior of the corners, so that the full FS displays the same instability as the corners. Thus, if the FS corners develop d-wave superconductivity, they induce d-wave superconductivity on the rest of the FS also.

Next, we extend the calculations away from the limit of weak coupling. Guided by our earlier analysis of the weak coupling problem, we assume that it is sufficient to determine the leading instability of the FS corners, since the rest of the FS will be dragged along. We derive the one loop RG equations for the corners, including correction terms coming from the edge fermions. These corrections are subleading in logs, however, they must be taken into account when interactions are not weak. We show that whereas at weak coupling there is only one stable fixed trajectory, above a critical coupling strength a second stable fixed trajectory appears. Thus, at weak coupling there is a unique instability (corresponding to d-wave superconductivity), whereas above a critical coupling strength there are two possible instabilities, with the nature of the microscopic interactions determining which one develops. The two instabilities are shown to correspond to d-wave superconductivity and ferromagnetism, respectively.

A. The model

For definiteness, in thissection, we focus on a honeycomb lattice. Fermions on a triangular lattice show the same behavior. We consider a system with nearest-neighbor hopping, described by the dispersion given by Eq. (33). We focus on van Hove filling at 5/8 density (a positive μ) and consider only the band of low-energy fermions. We have

$$\varepsilon_{\mathbf{k}} = -t\sqrt{1 + 4\cos\frac{k_y\sqrt{3}}{2}\cos\frac{3k_x}{2} + 4\cos^2\frac{k_y\sqrt{3}}{2}} - \mu.$$
(53)

The saddle point corresponds to setting the chemical potential $\mu = t$. The FS takes the form of a hexagon inscribed within a hexagonal BZ. The corners of the hexagonal FS are saddle points of the dispersion, and dominate the DOS.

We split up the FS into three inequivalent corners (labelled A, B, and C), and six inequivalent edges, labeled $\pm 1, \pm 2, \pm 3$ as shown in Fig. 19. Crystal momentum conservation strongly restricts the allows scattering processes. The allowed scattering
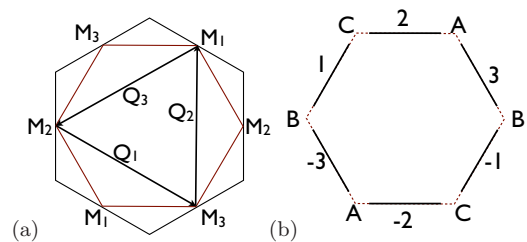

FIG. 19. (Color online) (a) Shows hexagonal FS inscribed within hexagonal BZ. The three inequivalent corners of the FS, M_1, M_2, M_3 are saddle points of the dispersion and dominate the density of states. The FS displays three nesting vectors Q_1, Q_2 and Q_3. (b) The FS may be split into corner regions A, B, and C and edge regions $\pm 1, \pm 2, \pm 3$.

processes involving at least one fermion on edge 1 are enumerated in the table below. The equivalent scattering processes involving fermions on one of the other edges can be deduced by symmetry. We also enumerate the inequivalent corner-corner scattering processes involving corners A and B. The processes involving corner C can again be deduced by symmetry. Note that all these processes conserve momentum up to a reciprocal lattice vector.

We now study the evolution of these various couplings under perturbative RG. An RG framework is suitable for this problem, because the interactions are marginal at tree level, with ln corrections in perturbation theory. The presence of a logarithmic van Hove singularity in the density of states (DOS) means that the most divergent diagrams at n loop order in perturbation theory diverge as $\ln^{2n} \frac{1}{E}$ in the infrared. The perturbation theory breaks down once $g_0 \ln^2 \frac{\Lambda}{E} \sim O(1)$, where g_0 is the bare coupling and Λ is the ultraviolet cutoff for the theory. In the weak coupling regime $g_0 \ll 1$, we have $\ln \Lambda/E \gg 1$ at the limit of applicability of perturbation theory. Therefore diagrams subleading in powers of $\ln \Lambda/E$ can be ignored, and we can concentrate our attention on the most strongly divergent diagrams. In this limit, the leading divergences can be resummed into a $\ln^2$ RG.

The perturbation theory for the full FS contains "corner-corner" loops (taken into account in the patch model), and also "edge-edge loops" and "corner-edge" loops (see Table I for a list of all the allowed scattering processes). We find that edge-edge and corner-edge loops are at most $\ln^1$ divergent. Thus they can be safely ignored in the weak coupling limit, but they can introduce $\ln^1$ corrections as we move away from weak coupling. Moreover, corner-edge loops are suppressed by a factor of Λ/W, where W is the bandwidth ($W \sim 12$ eV in graphene), and we assume $\Lambda \ll t$. We therefore neglect corner-edge loops throughout this paper. It thus follows that the $\ln^2$ RG is controlled by corner-corner loops, with $\ln^1$ corrections coming from corner-corner and edge-edge loops.

We present the analysis in two sections: first, we calculate the full FS RG in the weak coupling limit. In this limit, we can neglect subleading logarithms and concentrate on the $\ln^2$ divergent diagrams, which come from corner-corner loops only. We will show that in this limit the only instability is to d-wave superconductivity. Next, we extend the analysis away from weak coupling, by taking into account subleading $\ln^1$ corrections. We will show that above a critical coupling strength there appears a second instability, which corresponds to ferromagnetism. There is also the possibility of a spin density wave instability (SDW), but this requires us to stop the RG at some scale, since if the RG is allowed to run indefinitely some other instability ultimately overtakes the SDW. This picture becomes even more diverse for the case of strong nearest-neighbor interactions [36].

B. Full FS RG at weak coupling

The building blocks of the RG are particle-particle ladders and particle-hole bubbles, evaluated at momentum transfer zero and momentum transfer equal to a nesting vector. The ladders and bubbles involving corner fermions were presented in Ref. [25]. Here, we present ladders and bubbles involving edge fermions.

For diagrams involving only edge fermions, the leading divergence is logarithmic. There are no $\ln^2$ divergences because there are no saddle points on the edge. The ln divergences in edge-edge diagrams arise only in the Cooper and Pierls channels, i.e., in the particle-particle ladder at zero momentum, and in the particle-hole bubble at momentum equal to one nesting vector. These take the form

$$\Pi_{pp}^{\text{edge}}(0) = 2c\xi, \quad \Pi_{ph}^{\text{edge}}(Q) = 2c\xi,$$

where c is a cutoff dependent nonuniversal prefactor of order 1 and we have defined the RG scale $\xi = \frac{1}{2} \nu_0 \ln \frac{\Lambda}{E}$, which is equal to one half the density of states at an energy E.

TABLE I. Table listing allowed scattering processes. Here, σ, σ' are spin labels, A, B, C label inequivalent saddle points (FS corners), and $\pm 1, \pm 2, \pm 3$ label FS edges. The allowed interactions are assumed to be short range (i.e., they are assumed to have no momentum dependence).

Corner-corner	Incoming state	Outgoing state	Edge-edge	Incoming state	Outgoing state
g_1	$\|(A,\sigma),(B,\sigma')\rangle$	$\|(B,\sigma),(A,\sigma')\rangle$	h_{1A}	$\|(1,\sigma),(2,\sigma')\rangle$	$\|(2,\sigma),(1,\sigma')\rangle$
g_2	$\|(A,\sigma),(B,\sigma')\rangle$	$\|(A,\sigma),(B,\sigma')\rangle$	h_{1A}	$\|(1,\sigma),(-3,\sigma')\rangle$	$\|(-3,\sigma),(1,\sigma')\rangle$
g_3	$\|(A,\sigma),(A,\sigma')\rangle$	$\|(B,\sigma),(B,\sigma')\rangle$	h_{1B}	$\|(1,\sigma),(3,\sigma')\rangle$	$\|(3,\sigma),(1,\sigma')\rangle$
g_4	$\|(A,\sigma),(A,\sigma')\rangle$	$\|(A,\sigma),(A,\sigma')\rangle$	h_{1B}	$\|(1,\sigma),(-2,\sigma')\rangle$	$\|(-2,\sigma),(1,\sigma')\rangle$
Corner-Edge	Incoming state	Outgoing state	h_{1C}	$\|(1,\sigma),(-1,\sigma')\rangle$	$\|(-1,\sigma),(1,\sigma')\rangle$
v_{1A}	$\|(1,\sigma),(B,\sigma')\rangle$	$\|(B,\sigma),(1,\sigma')\rangle$	h_{2A}	$\|(1,\sigma),(2,\sigma')\rangle$	$\|(1,\sigma),(2,\sigma')\rangle$
v_{1A}	$\|(1,\sigma),(C,\sigma')\rangle$	$\|(C,\sigma),(1,\sigma')\rangle$	h_{2A}	$\|(1,\sigma),(-3,\sigma')\rangle$	$\|(1,\sigma),(-3,\sigma')\rangle$
v_{1B}	$\|(1,\sigma),(A,\sigma')\rangle$	$\|(A,\sigma),(1,\sigma')\rangle$	h_{2B}	$\|(1,\sigma),(-2,\sigma')\rangle$	$\|(1,\sigma),(-2,\sigma')\rangle$
v_{2A}	$\|(1,\sigma),(B,\sigma')\rangle$	$\|(1,\sigma),(B,\sigma')\rangle$	h_{2B}	$\|(1,\sigma),(3,\sigma')\rangle$	$\|(1,\sigma),(3,\sigma')\rangle$
v_{2A}	$\|(1,\sigma),(C,\sigma')\rangle$	$\|(1,\sigma),(C,\sigma')\rangle$	h_{2C}	$\|(1,\sigma),(-1,\sigma')\rangle$	$\|(1,\sigma),(-1,\sigma')\rangle$
v_{2B}	$\|(1,\sigma),(A,\sigma')\rangle$	$\|(1,\sigma),(A,\sigma')\rangle$	h_3	$\|(1,\sigma),(1,\sigma')\rangle$	$\|(-1,\sigma),(-1,\sigma')\rangle$
v_{3A}	$\|(1,\sigma),(-1,\sigma')\rangle$	$\|(B,\sigma),(B,\sigma')\rangle$	h_4	$\|(1,\sigma),(1,\sigma')\rangle$	$\|(1,\sigma),(1,\sigma')\rangle$
v_{3A}	$\|(1,\sigma),(-1,\sigma')\rangle$	$\|(C,\sigma),(C,\sigma')\rangle$	h_5	$\|(1,\sigma),(-1,\sigma')\rangle$	$\|(2,\sigma),(-2,\sigma')\rangle$
v_{3B}	$\|(1,\sigma),(-1,\sigma')\rangle$	$\|(A,\sigma),(A,\sigma')\rangle$	h_5	$\|(1,\sigma),(-1,\sigma')\rangle$	$\|(-3,\sigma),(3,\sigma')\rangle$
v_4	$\|(1,\sigma),(B,\sigma')\rangle$	$\|(-1,\sigma),(C,\sigma')\rangle$	h_6	$\|(1,\sigma),(-1,\sigma')\rangle$	$\|(-2,\sigma),(2,\sigma')\rangle$
v_4	$\|(1,\sigma),(C,\sigma')\rangle$	$\|(-1,\sigma),(B,\sigma')\rangle$	h_6	$\|(1,\sigma),(-1,\sigma')\rangle$	$\|(3,\sigma),(-3,\sigma')\rangle$
v_5	$\|(1,\sigma),(B,\sigma')\rangle$	$\|(C,\sigma),(-1,\sigma')\rangle$			
v_5	$\|(1,\sigma),(C,\sigma')\rangle$	$\|(B,\sigma),(-1,\sigma')\rangle$			

The above expressions assume perfect nesting. Imperfect nesting may be dealt with by cutting off the growth of $\Pi_{ph}(Q)$ at some RG scale ξ_c, as discussed in Ref. [25]. All other edge-edge diagrams are convergent. Meanwhile, it may be straightforwardly verified that all ladders and bubbles constructed out of one corner fermion and one edge fermion are suppressed by Λ/W, where, we remind, W is the bandwidth and Λ is the UV cutoff for the RG. The suppression arises because a corner-edge pair can never be nested in any scattering channel, and thus the phase space for these scattering processes is strongly restricted. We assume $\Lambda/W \ll 1$, which allows us to neglect mixed corner-edge loops. Moreover, in the weak coupling limit, $\ln^2$ divergent diagrams are much more important than $\ln$ divergent diagrams, which also allows us to neglect edge-edge loops. The resulting $\ln^2$ renormalizations come only from diagrams with corner-corner loops. The RG equations in the corner-corner sector are

$$\frac{dg_1}{d\xi} = 2d_1 g_1(g_2 - g_1), \quad \frac{dg_2}{d\xi} = d_1\left(g_2^2 + g_3^2\right),$$

$$\frac{dg_3}{d\xi} = -d_0\left[(n-2)g_3^2 + 2g_3 g_4\right] + 2d_1 g_3(2g_2 - g_1), \quad (54)$$

$$\frac{dg_4}{d\xi} = -d_0\left[(n-1)g_3^2 + g_4^2\right].$$

Here, d_0 and the d_1 are functions of ξ and we have defined

$$d_0(\xi) = \frac{d\Pi_{pp}^{\text{corner}}(0)}{d\xi} = \frac{\xi + \xi_0}{2},$$
$$\qquad\qquad\qquad\qquad\qquad\qquad (55)$$
$$d_1(\xi) = \frac{d\Pi_{ph}^{\text{corner}}(Q)}{d\xi} = \frac{\xi + \xi_0}{2},$$

where perfect nesting is assumed. Imperfect nesting may be dealt with by taking $d_1 < d_0$, as discussed in Ref. [25]. We have also defined $\xi_0 = \frac{1}{2}\nu_0 \ln W/\Lambda$, and we assume that the UV cutoff Λ (and hence ξ_0) is the same for d_1 and d_0.

Meanwhile, we find that for the edge-edge couplings,

$$\frac{dh_{1A(B)}}{d\xi} = O(\xi^0),$$

$$\frac{dh_{1C}}{d\xi} = -2v_{3A}^2 d_0 - v_{3B}^2 d_0 - 2v_4^2 d_1 + O(\xi^0).$$

$$\frac{dh_{2A(B)}}{d\xi} = O(\xi^0),$$

$$\frac{dh_{2C}}{d\xi} = -2v_{3A}^2 d_0 - v_{3B}^2 d_0 + v_4^2 d_1 + O(\xi^0),$$

$$\frac{dh_3}{d\xi} = v_5^2 d_1 - 2v_4^2 d_1 + O(\xi^0), \quad \frac{dh_4}{d\xi} = O(\xi^0),$$

$$\frac{dh_5}{d\xi} = -v_3^2 d_0 - 2v_{3A}v_{3B} d_0 + O(\xi^0),$$

$$\frac{dh_6}{d\xi} = -2v_{3A}v_{3B} d_0 + O(\xi^0).$$

We emphasize that there are $\ln$ square divergences in the β functions coming from corner-corner loops, because of which d_1 and d_0 grow with ξ as $d_{0,1} \sim \xi$. This allows us to asymptotically neglect corrections to the β functions which do not grow with ξ [denoted above as $O(\xi^0)$ corrections].

Finally, for the corner-edge couplings,

$$\frac{dv_{1A(B)}}{d\xi} = O(\xi^0), \quad \frac{dv_{2A(B)}}{d\xi} = O(\xi^0),$$

$$\frac{dv_{3A}}{d\xi} = -2v_{3A}(g_4 + g_3)d_0 - 2v_{3B}g_3 d_0 + O(\xi^0),$$

$$\frac{dv_{3B}}{d\xi} = -2v_{3B}g_4 d_0 - 4v_{3A}g_3 d_0 + O(\xi^0), \quad (56)$$

$$\frac{dv_4}{d\xi} = -4v_4 g_3 d_1 + O(\xi^0),$$

$$\frac{dv_5}{d\xi} = 2v_5 g_2 d_1 + 2v_4 g_1 d_1 + O(\xi^0).$$

We can now solve the system sequentially. First, we solve the corner system in a leading log approximation. The corner-corner couplings diverge along a fixed trajectory with $g_{1,2,3} \to \infty, g_4 \to -\infty$ and $|g_4| > g_3 > g_2 \gg g_1$. We can now determine what happens in the corner-edge coupling space. It is convenient to define $v_+ = 2v_{3A} + v_{3B}$ and $v_- = v_{3A} - v_{3B}$. We find that v_5 and v_- are relevant and flow to $+\infty$ (with $v_- > v_5$) whereas the rest of the corner-edge coupling sector is irrelevant. Feeding this into the edge sector, we see that

$$\frac{dh_{1C}}{d\xi} = \frac{dh_{2c}}{d\xi} = -\frac{2}{3}v_-^2 d_0, \quad \frac{dh_3}{d\xi} = v_5^2 d_1,$$

$$\frac{dh_5}{d\xi} = \frac{1}{3}v_-^2 d_0, \quad \frac{dh_6}{d\xi} = \frac{4}{9}v_-^2 d_0.$$

with the rest of the edge-edge sector being irrelevant. Thus we see that $h_{3,5,6} \to \infty$, $h_{1C,2C} \to -\infty$ and all other edge-edge couplings flow to zero.

We now wish to calculate the susceptibilities for the full FS. In Ref. [25], we already analyzed the susceptibilities of the corners. We now calculate the susceptibilities towards various ordering types for the FS edges. We illustrate the procedure by calculating the susceptibilities towards superconductivity. We introduce test vertices corresponding to Cooper pairing at zero crystal momentum. There are six vertices corresponding to six inequivalent ways of making Cooper pairs $\Delta_{1-1}, \Delta_{-11}, \Delta_{2-2}, \Delta_{-22}, \Delta_{3-3}, \Delta_{-33}$, where it follows from Hermiticity that $\Delta_{1-1} = \Delta_{-11}^*$. We now calculate the renormalization of these six test vertices under RG. This is governed by a martix equation $\frac{d\Delta}{d\xi} = H\Delta$, where Δ is a six component vector of test vertices and the matrix H is

$$H = -\begin{pmatrix} h_{2c} & h_5 & h_6 & h_{1C} & h_6 & h_5 \\ h_5 & h_{2C} & h_5 & h_6 & h_{1C} & h_6 \\ h_6 & h_5 & h_{2C} & h_5 & h_6 & h_{1c} \\ h_{1C} & h_6 & h_5 & h_{2C} & h_5 & h_6 \\ h_6 & h_{1C} & h_6 & h_5 & h_{2C} & h_5 \\ h_5 & h_6 & h_{1C} & h_6 & h_5 & h_{2C} \end{pmatrix}. \quad (57)$$

The most positive eigenvalue (corresponding to the strongest instability), given the asymptotic values of the h fields, happens for the eigenvectors $(-1, 0, 1, -1, 0, 1)$ and $(1, -2, 1, 1, -2, 1)$, which correspond to the two d-wave channels d_{xy} and $d_{x^2-y^2}$. The eigenvalue $2(h_{1C} + h_{2C} - h_5 - h_6)$

is the exponent with which the d-wave superconducting instability diverges.

An analogous analysis for SDW yields an exponent of $2(h_{1C} + h_{2C})$. This is an exponent smaller than the corresponding exponent for d-wave superconductivity. Thus SDW is subleading to d-wave superconductivity even on the edges.

We thus obtain the pleasing result that when d-wave superconductivity is the leading instability at the FS corners, it is also the leading instability at the edges. Put another way, the corners "pull" the edges along into the superconducting phase.

C. RG away from weak coupling

We now extend the RG away from weak coupling. When deriving the RG equations away from weak coupling, one must keep track of ln and $\ln^2$ divergent terms. In the weak coupling limit, the $\ln^2$ divergences are parametrically stronger, and control the flow. However, when interactions are of moderate strength, the phase transition can set in when ln is of order one, at which point there is no distinction between ln and $\ln^2$ terms. Therefore, to determine the phase structure away from weak coupling, we must keep track of ln and $\ln^2$ divergences.

As we have discussed, while $\ln^2$ divergences come from corner-corner loops only, $\ln^1$ divergences arise also from edge-edge loops. Corner-edge loops are parametrically supressed by $\Lambda/t \ll 1$, and may be ignored. We present the full RG away from weak coupling in two steps. First, we analyze what happens if we ignore edge fermions altogether. Then we put the edge fermions back in.

D. Patch RG away from weak coupling

The RG equations for the corner-corner sector are obtained by extending the approach developed for the square lattice problem [37] to the number of patches $n > 2$. The number of patches matters only in diagrams with zero net momentum in fermion loops, since it is only there that we get summation over fermion flavors inside the loop. In this manner, we obtain the beta functions:

$$\frac{dg_1}{d\xi} = 2d_1 g_1(g_2 - g_1) + d_2 g_1[2g_4 + (n-2)g_1] - 2d_3 g_1 g_2,$$

$$\frac{dg_2}{d\xi} = d_1(g_2^2 + g_3^2) + 2d_2[g_1 g_4 + (n-2)(g_1 g_2 - g_2^2)$$
$$- g_2 g_4] - d_3(g_1^2 + g_2^2),$$

$$\frac{dg_3}{d\xi} = -(n-2)d_0 g_3^2 - 2d_0 g_3 g_4 + 2d_1 g_3(2g_2 - g_1),$$

$$\frac{dg_4}{d\xi} = -(n-1)d_0 g_3^2 - d_0 g_4^2 + d_2[(n-1)g_1^2$$
$$+ 2(n-1)(g_1 g_2 - g_2^2) + g_4^2]. \tag{58}$$

Following the notations first introduced in Ref. [37] for RG studies of the square lattice, we have defined

$$d_0 = \frac{\partial \Pi_{pp}(Q)}{\partial \xi} = \frac{\xi_0 + \xi}{2}, \quad d_0 = \frac{\partial \Pi_{ph}(Q)}{\partial \xi} \approx \frac{\xi_0 + \xi}{2},$$

$$d_2 = \frac{\partial \Pi_{ph}(0)}{\partial \xi} = 1, \quad d_3 = \frac{\partial \Pi_{pp}(Q)}{\partial \xi} \leqslant 1, \tag{59}$$

where $\xi_0 = \frac{1}{2}\nu_0 \ln\frac{\Lambda_0}{\Lambda}$ and we have assumed perfect nesting. We have allowed for the UV cutoff of our theory, Λ, being different from the scale at which the dispersion changes, Λ_0.

There are two qualitatively different regimes. When the bare interactions are weak at the UV scale, the RG does not flow to strong coupling until a very large scale ξ_c, such that $d_2(\xi_c) \ll 1$, $d_3(\xi_c) \ll 1$. In this limit, the $\ln^1$ terms in the β functions can be neglected, and the phase structure is controlled by the $\ln^2$ divergent terms, i.e., we can set $d_2 = 0, d_3 = 0$. The system of RG equations collapses onto the system studied in Ref. [25], and the only possible phase that can result for the corner fermions is d-wave superconductivity.

A qualitatively different behavior is obtained when interactions are stronger. When the flow to strong coupling occurs for $\ln \sim O(1)$, there is no difference between ln and $\ln^2$ terms, and both must be taken into account simultaneously. To understand the behavior in this regime, we set $d_0 = d_1 = d_2 = d_3 = 1$. This places $\ln^2$ and ln divergent terms on an equal footing. Defining $g_i' = dg_i/d\xi$, we obtain the RG equations (for $n = 3$)

$$\begin{aligned} g_1' &= g_1(2g_4 - g_1), \\ g_2' &= g_3^2 - g_1^2 + 2(g_2 + g_4)(g_1 - g_2), \\ g_3' &= g_3(4g_2 - 2g_1 - 2g_4 - g_3), \\ g_4' &= 2g_1^2 - 2g_3^2 + 4g_2(g_1 - g_2). \end{aligned} \tag{60}$$

This has finite coupling fixed points along the line $g_1 = g_2 = g_3 = 0$ and also along the line $g_1 = g_2 = g_3 = 2g_4$. To investigate the stability of these finite coupling solutions, we consider small deviations from the fixed line, δg_i, where $i = 1, 2, 3, 4$. The flow of these small deviations is governed by $\delta g_i' = K_{ij} \delta g_j$, where the matrix K is given by

$$K = 2 \begin{bmatrix} -g_1 + g_4 & 0 & 0 & g_1 \\ g_2 + g_4 - g_1 & g_1 - 2g_2 - g_4 & g_3 & g_1 - g_2 \\ -g_3 & 2g_3 & -g_3 + 2g_2 - g_1 - g_4 & -g_3 \\ 2g_1 + 2g_2 & g_1 - 4g_2 & -2g_3 & 0 \end{bmatrix}. \tag{61}$$

The fixed line is stable only if all the eigenvalues of K are negative (or zero). However, K has at least one positive eigenvalue for both $g_1 = g_2 = g_3$ and $g_1 = g_2 = g_3 = 2g_4$, therefore both fixed lines are unstable. The only stable fixed points of the flow are at infinity.

To determine the possible fixed trajectories, we substitute into Eq. (60) the scaling ansatz

$$g_i(\xi) = \frac{G_i}{\xi_c - \xi}, \tag{62}$$

where ξ_c is the RG time at which the couplings diverge. This turns the four coupled differential equations Eq. (60) into four coupled algebraic equations, which can be solved on mathematica. The equations are

$$
\begin{aligned}
G_1 &= G_1(2G_4 - G_1), \\
G_2 &= G_3^2 - G_1^2 + 2(G_2 + G_4)(G_1 - G_2), \\
G_3 &= G_3(4G_2 - 2G_1 - 2G_4 - G_3), \\
G_4 &= 2G_1^2 - 2G_3^2 + 4G_2(G_1 - G_2).
\end{aligned}
\tag{63}
$$

The scaling equations (63) are solved most simply by $G_1 = G_2 = G_3 = G_4 = 0$, however, this noninteracting fixed point lies on the two fixed lines that were investigated above, and which were found to be unstable. Therefore we can neglect this trivial solution.

We find using mathematica that there are 13 distinct nontrivial solutions of (63), corresponding to 13 different limiting trajectories. However, not all of them can be accessed starting from repulsive interactions. From Eq. (60), we note that the β functions for g_1 and g_3 vanish when the respective couplings go to zero. Thus these couplings cannot change sign, and we can exclude any solution corresponding to negative values for g_1 or g_3. Similarly, $2g_2' + g_4' \propto 2g_2 + g_4$, therefore the combination of couplings $2g_2 + g_4$ also cannot change sign, and we can exclude any solution with $2g_2 + g_4 < 0$. These conditions allow us to eliminate nine of the thirteen solutions to leave us with only four fixed trajectories that can be accessed starting from repulsive interactions. The four solutions correspond to values $(G_1, G_2, G_3, G_4) = (0, \frac{1}{2}, 0, -1), (0, \frac{1}{6}, \frac{1}{3}, -\frac{1}{3}), (\frac{1}{2}, \frac{1}{4}, 0, \frac{3}{4})$, or $(3, -1, 0, 2)$.

We further want to determine which of these fixed trajectories are stable. We therefore consider small deviations from the fixed trajectory,

$$
g(\xi) = \frac{G_i}{\xi_c - \xi} + \delta g_i.
\tag{64}
$$

Substituting into Eq. (60) and linearizing, we obtain a flow equation of the form $(\xi_c - \xi)\delta g_i' = K_{ij}\delta g_j$, where K is given by Eq. (61) with $g_i \to G_i$.

Again, we want to use the matrix K to check the stability of the fixed trajectories. However, the matrix K will now certainly

have at least one eigenvector with positive eigenvalue—the eigenvector corresponding to flow along the fixed trajectory. We want to exclude this direction from our stability analysis. Therefore we project onto the subspace orthogonal to the fixed trajectory by multiplying by the projection matrix $P = 1 - (G_1, G_2, G_3, G_4) \otimes (G_1, G_2, G_3, G_4)^T$. We then examine the eigenvalues of the matrix KP. If this matrix has any positive eigenvalues, then the fixed trajectory is unstable. This stability analysis reveals that there are only two stable fixed trajectories that can be accessed starting from repulsive interactions, corresponding to two possible phases. These fixed trajectories have critical couplings $(G_1, G_2, G_3, G_4) = (0, \frac{1}{6}, \frac{1}{3}, -\frac{1}{3})$ and $(\frac{1}{2}, \frac{1}{4}, 0, \frac{3}{4})$, respectively. From a numerical solution of the differential equations (60), we have confirmed that the RG does indeed converge to one of these two fixed trajectories.

It now remains to determine what the leading instability is along each fixed trajectory. We consider pairing in all channels, ln divergent as well as $\ln^2$ divergent (since we have set $d_1 = d_2 = d_3 = d_4 = 1$, there is no difference between these ordering channels). We now consider the susceptibility towards developing a nonzero expectation value for every possible fermion bilinear, i.e., particle-particle pairing and particle hole pairing, at momentum transfer zero or momentum transfer Q, in the spin singlet or spin triplet channel, and with any possible structure in patch space. The various susceptibilities are tabulated in Table II.

We observe that the two fixed points show very different behavior. At the first fixed point, there are instabilities in the (doubly degenerate) d-wave pairing channel, in the SDW channel, and in the d-wave Pomeranchuk channel, with the superconducting instability leading. Thus this fixed point is adiabatically connected to the weak coupling fixed point, which also exhibits a leading instability to (doubly degenerate) d-wave superconductivity.

Meanwhile, at the second fixed point, there are instabilities in the finite momentum pairing channel and in the SDW channel, and also in the ferromagnet channel, with both s- and d-wave symmetry. The leading instability is in the isotropic (s-wave) ferromagnet channel. The resulting state breaks spin rotation symmetry but preserves lattice rotation symmetry and

TABLE II. Susceptibilities to various kinds of order scale as $(\xi_c - \xi)^\alpha$, with $\alpha < 0$ indicating an instability. We present here the susceptibilities to various types of order at each fixed point, calculated for $d_1 = d_2 = d_3 = 1$, i.e., no difference between ln and $\ln^2$ divergent ordering channels. Here, $c^\dagger$ is an electron creation operator, with a number subscript 1,2,3 indicating which patch the electron is created on, and a subscript arrow labeling the spin state.

Ordering channel	Verbal description	Susceptibility exponent	$(0, \frac{1}{6}, \frac{1}{3}, -\frac{1}{3})$	$(\frac{1}{2}, \frac{1}{4}, 0, \frac{3}{4})$
$\langle c_{1\uparrow}c_{1\downarrow}\rangle = \Delta_1 = \Delta_2 = \Delta_3$	s-wave SC	$2(2G_3 + G_4)$	$\frac{2}{3}$	$\frac{3}{2}$
$\langle c_{1\uparrow}c_{1\downarrow}\rangle = \Delta_1 = -\Delta_3, \Delta_2 = 0$	d-wave SC(doubly degenerate)	$2(G_4 - G_3)$	$-\frac{4}{3}$	$\frac{3}{2}$
$\langle c_{1\uparrow}c_{2\downarrow}\rangle$	finite momentum pairing	$2(G_2 - G_1)$	$\frac{1}{3}$	$-\frac{1}{2}$
$\langle c_{1\uparrow}^\dagger c_{2\downarrow}\rangle$	SDW	$-2(G_2 + G_3)$	-1	$-\frac{1}{2}$
$\langle c_{1\uparrow}^\dagger c_{2\uparrow}\rangle$	CDW	$(2G_1 - G_2 + G_3)$	$\frac{1}{6}$	$\frac{3}{4}$
$\langle c_{1\uparrow}^\dagger c_{1\downarrow}\rangle = \Delta_1 = \Delta_2 = \Delta_3$	s-wave ferromagnet	$-2(G_4 + 2G_1)$	$\frac{2}{3}$	$-\frac{7}{2}$
$\langle c_{1\uparrow}^\dagger c_{1\downarrow}\rangle = \Delta_1 = -\Delta_3, \Delta_2 = 0$	d-wave ferromagnet (doubly degenerate)	$-2(G_4 - G_1)$	$\frac{2}{3}$	$-\frac{1}{2}$
$\langle c_{1\uparrow}^\dagger c_{1\uparrow}\rangle = \Delta_1 = \Delta_2 = \Delta_3$	charge compressibility	$4G_2 - 2G_1 + G_4$	$\frac{1}{3}$	$\frac{3}{4}$
$\langle c_{1\uparrow}^\dagger c_{1\uparrow}\rangle = \Delta_1 = -\Delta_3, \Delta_2 = 0$	d-wave Pomeranchuk (doubly degenerate)	$G_1 + G_4 - 2G_2$	$-\frac{2}{3}$	$\frac{3}{4}$

translation symmetry. Such a ferromagnet state is natural to expect in the vicinity of a van Hove singularity in the DOS. However, it is only accessible for not too weak bare couplings. In the limit of zero coupling strength, the leading instability is the $d + id$ superconductor.

E. Full FS RG away from weak coupling

Thus far we concentrated solely on the corner fermions. We now put the edge fermions back in. We assume in the interests of analytic tractability that the edge fermions are in the same phase as the corner fermions (we demonstrated this to be the case at weak coupling). The problem then simplifies to determining the leading instability of the corner fermions, taking into account the renormalizations arising from the edge fermions. Assuming that $d_0 = d_1 = d_2 = d_3 = c = 1$, so that all divergent diagrams in all channels are treated on an equal footing, and corner-corner loops and edge-edge loops are treated on the same footing also, we obtain β functions for the corner-corner sector, which take the form

$$
\begin{aligned}
g_1' &= g_1(2g_4 - g_1) - 2v_5^2, \\
g_2' &= g_3^2 - g_1^2 + 2(g_2 + g_4)(g_1 - g_2) + v_4^2, \\
g_3' &= g_3(4g_2 - 2g_1 - 2g_4 - g_3) - 2v_{3A}^2 - 4v_{3B}^2 + v_4^2 - 2v_5^2, \\
g_4' &= 2g_1^2 - 2g_3^2 + 4g_2(g_1 - g_2) - 4v_{3A}^2 - 2v_{3B}^2.
\end{aligned}
\tag{65}
$$

We make one final approximation. Namely, in the β functions for the corner-edge couplings, we retain only $\ln^2$ divergent terms arising from corner-corner loops, and neglect terms of $O(\ln^1)$. The RG equations for the corner-edge couplings are then given by Eq. (56). Again, we solve the system sequentially. First, we solve for the g couplings. Then we solve for the v couplings. Finally, we determine the back-action of the v on the g couplings.

We note that the couplings v_4 and $2v_{3A} + v_{3B}$ are always irrelevant. The coupling $v_5 \to \infty$ is the only relevant corner-edge coupling along the ferromagnetic trajectory, whereas the couplings v_5 and $v_- = v_{3A} - v_{3B}$ are both relevant along the d-wave superconducting trajectory. Along the ferromagnetic trajectory, neglecting the irrelevant couplings, we obtain

$$
\begin{aligned}
g_1' &\approx g_1(2g_4 - g_1) - 2v_5^2, \\
g_2' &\approx g_3^2 - g_1^2 + 2(g_2 + g_4)(g_1 - g_2), \\
g_3' &\approx g_3(4g_2 - 2g_1 - 2g_4 - g_3) - 2v_5^2, \\
g_4' &\approx 2g_1^2 - 2g_3^2 + 4g_2(g_1 - g_2).
\end{aligned}
\tag{66}
$$

Thus, along the ferromagnetic trajectory, the corner-edge couplings affect only the g_1 and g_3 couplings. They tend to suppress the g_1 coupling, thereby suppressing ferromagnetism, and they can also drive g_3 negative. If g_3 changes sign, then a number of other phases, such as s-wave superconductivity and charge density waves, become possible. Thus the effect of edge fermions can be quite marked along the ferromagnetic sector, where they can alter the dominant phase from ferromagnetism to something else, like CDW or s-wave superconductivity. However, this will only happen if the effect of edge fermions is sufficiently strong, which requires strong couplings.

Meanwhile, along the SCd trajectory, both v_5 and $v_- = v_{3A} - v_{3B}$ are relevant. The resulting equations, neglecting

irrelevant corrections, are

$$
\begin{aligned}
g_1' &= g_1(2g_4 - g_1) - 2v_5^2, \\
g_2' &= g_3^2 - g_1^2 + 2(g_2 + g_4)(g_1 - g_2), \\
g_3' &= g_3(4g_2 - 2g_1 - 2g_4 - g_3) - 2v_-^2 - 2v_5^2, \\
g_4' &= 2g_1^2 - 2g_3^2 + 4g_2(g_1 - g_2) - \tfrac{4}{3}v_-^2.
\end{aligned}
\tag{67}
$$

Thus the edge fermions suppress g_3, which suppresses SCd and SDW equally, but they also make g_4 more negative, which strengthens superconductivity. Thus the effect of edge fermions along the SCd trajectory is to strengthen superconductivity with respect to SDW. Of course, if couplings are sufficiently strong that the edge fermions trigger a sign change in g_1, then an entirely new phase could arise. A CDW phase would be the most likely candidate given a negative g_1.

Thus we see that along the edge fermions can destabilise the ferromagnetic trajectory towards other phases, like s-wave superconductivity and CDW. Meanwhile, along the SCd trajectory, edge fermions strengthen superconductivity with respect to SDW. However, they can also induce formation of a different kind of phase, such as a CDW.

F. Summary of the system behavior at the van Hove point

Thus we can make the following conclusions. (1) In the weak coupling limit, the full FS RG reproduces exactly the patch RG for the saddle points presented in Ref. [25]. The entire FS enters the same phase as the FS corners, which is a d-wave superconductor. (2) Once we move away from weak coupling, the RG approach is no longer controlled, and the neglect of higher loop diagrams can no longer be justified. However, the procedure can still be applied, although the results must be treated with caution. (3) Away from weak coupling, a patch RG analysis that focuses purely on the hexagon corners reveals two distinct instabilities: one to d-wave superconductivity, and another to ferromagnetism. The SDW is never the leading instability if the RG is allowed to run indefinitely, but it may dominate if the RG is stopped at some intermediate energy scale by higher loop effects or self energy effects. The ferromagnetic phase is the principal new result from extending the patch RG to strong coupling. (4) The effect of the edge fermions at strong coupling can also be estimated. Along the ferromagnetic trajectory, the edge fermions suppress ferromagnetism, and may destabilize it in the strong coupling limit towards a different phase, like a CDW or an s-wave superconductor. Meanwhile, along the SCd trajectory, the edge fermions strengthen SCd with respect to SDW, but they may destabilise SCd at strong coupling towards another phase, such as a CDW.

Note, however, that although van Hove singularities arise rather generically (see, e.g., Ref. [38]), for most of them the divergence in the density of states either is not accompanied by Fermi surface nesting, due to, e.g., the presence of longer-range hybridization, or the nesting vector is not one half of a reciprocal lattice vector. In these cases, the physics differs quite substantially from the discussions in this paper. For further details see, e.g., Refs. [39–41].

V. EXPERIMENTAL OUTLOOK

Despite its rapid development in recent years, the investigation of unconventional superconductivity in systems on hexagonal lattices is still at an early stage [18]. A core challenge for hexagonal scenarios in general is to identify whether superconductivity is of electronic origin. Because many hexagonal systems exhibit a strong propensity to lattice distortions, phonon mediated *s*-wave superconductivity is often a valid competitor.

With respect to electronically mediated superconductivity, one primary direction is a search for a potential chiral *d*-wave pairing in graphene doped to the van Hove point [25,27,28,32]. Such doping can be reached by chemical means, as Ref. [42] has demonstrated. It will be revealing to conduct low-temperature transport experiments capable of detecting superconductivity on these samples. Given the large amounts of disorder introduced by chemical doping, however, it is not clear that superconductivity should arise in chemically doped graphene. Alternative doping techniques, such as ionic liquid gating, which introduce less disorder, have not yet succeeded in reaching van Hove filling.

However, as elaborated on in our paper and also in earlier publications [20,27], even well away from the van Hove point, there is a possibility for triplet (*f*-wave) superconductivity. Thus another primary direction is fabrication of materials that are doped less that all the way to the van Hove point, but have a smaller amount of disorder. Low-temperature transport experiments on such samples are highly desirable.

With ongoing material research fostering the hope for further compounds to arise, there are already several promising hexagonal systems exhibiting unconventional superconductivity which might be describable along the analysis laid out in this paper. An interesting candidate material is SrPtAs [43], where preliminary experimental evidence indicates a nonzero magnetic moment below T_c, combined with the absence of line nodes. In particular, nuclear resonance experiments seem to be consistent with chiral *d*-wave superconductivity [44].

Organic charge-transfer complexes such as the Bechgaard salts [33,45], the layered triangular superconductors κ-(BEDT-TTF)$_2 X$ [46], and the water-intercalated sodium cobaltates [39,47] are triangular lattice compounds, which, according to our study, should display *d*-wave and *f*-wave superconductivity at different dopings. While the interaction over bandwidth ratio is rather high in these materials, the insights from Kohn-Luttinger and parquet-RG considerations, favoring unconventional superconductivity, might still be valuable.

Artificial hexagonal optical lattices loaded with fermionic isotopes of ultracold atomic gases could establish another realization in nature of the scenarios we describe in this paper. While the challenge is to reduce the effective temperature $T/T_{\rm F}$ to make the Fermi surface instabilities accessible, all other parameters are likely to be easily matched with an outset that tends to exhibit unconventional superconductivity [48].

VI. CONCLUSIONS

We have studied the emergence of superconductivity in hexagonal lattice systems (both honeycomb and triangular) over a wide range of doping levels. Away from van Hove doping, the Kohn-Luttinger framework provides a satisfactory formalism for investigating the emergence of superconductivity. Superconductivity arises if the attraction generated in a particular channel at second order in perturbation theory exceeds the bare repulsion in the corresponding channel. Thus Kohn-Luttinger superconductivity at generic doping levels in a hexagonal lattice system is a threshold phenomenon, and moreover depends on the details of the lattice scale interactions. We find that in a pure Hubbard model, superconductivity arises very generally, whereas including further neighbor interactions disfavors superconductivity. However, we also find that, if superconductivity does arise at a generic doping, it is likely to be in the *f*-wave channel. Thus hexagonal lattice systems are expected to provide a good platform for the *f*-wave superconductivity, which as far as we know has never yet been observed.

Meanwhile, close to van Hove filling, the Kohn-Luttinger formalism is inadequate, owing to the divergence of perturbation theory, and also because of the nesting of the Fermi surface, which strongly couples the particle-particle and particle-hole channels. We have constructed and analyzed a parquet RG, which provides an asymptotically exact description of the physics at weak coupling. The parquet analysis introduced in this paper includes the full Fermi surface in the calculation, unlike [25], which concentrated on the parts of the Fermi surface close to the saddle points. The full Fermi surface parquet RG confirms the conclusions of Ref. [25], establishing that the weak coupling physics is highly universal, with any choice of bare repulsive interactions producing an instability to doubly degenerate *d*-wave superconductivity. Moreover, the feedback of particle hole channels into the particle-particle sector ensures that the critical temperature is strongly enhanced over the Kohn-Luttinger estimates. Meanwhile, extending the analysis away from weak coupling, we find that the main competitors to superconductivity if interactions are not that weak are ferromagnetism, or, potentially, charge density waves.

We expect the ideas laid out in this paper will be relevant for all investigations of superconductivity in hexagonal lattice systems. We note in particular that chiral *d*-wave superconductivity may already have been observed in SrPtAs [43], in the vicinity of van Hove doping. We hope that other ideas discussed above, such as *f*-wave pairing away from van Hove doping, will also be observed in the not too distant future.

Note added. It was brought to our attention after the completion of this work that the emergence of *f*-wave triplet pairing on a triangular lattice was also discussed in Ref. [49] in the context of superconductivity in $Na_{0.35}CoO_2 \cdot 1.3H_2O$. These authors included terms of order U^3 and argued that these terms increase T_c for *f*-wave pairing.

ACKNOWLEDGMENTS

[1] A. A. Abrikosov, L. P. Gorkov, and I. Y. Dzyaloshinskii, *Quantum Field Theoretical Methods in Statistical Physics* (Dover, New York, 1975).

[2] W. Kohn and J. M. Luttinger, Phys. Rev. Lett. **15**, 524 (1965).

[3] R. Shankar, Rev. Mod. Phys. **66**, 129 (1994); W. Metzner, C. Castellani, and C. Di Castro, Adv. Phys. **47**, 317 (1998).

[4] S. Maiti and A. V. Chubukov, *Superconductivity from Repulsive Interactions*, edited by A. Avella and F. Manchini, in Lectures on the Physics of Strongly Correlated Systems XVII (AIP, Melville, NY, 2013).

[5] A. J. Leggett, Rev. Mod. Phys. **47**, 331 (1975); R. Balian and N. R. Werthamer, Phys. Rev. **131**, 1553 (1963); P. W. Anderson and W. F. Brinkman, Phys. Rev. Lett. **30**, 1108 (1973).

[6] D. Vollhardt and P. Woelfle, *Superfluid Phases of Helium 3* (Taylor and Francis, London, 1990).

[7] J. G. Bednorz, K. A. Mueller, Zeitschrift für Physik B **64**, 189 (1986).

[8] D. J. Scalapino, Rev. Mod. Phys. **84**, 1383 (2012), and references contained therein.

[9] Y. Kamihara, T. Watanabe, M. Hirano, and H. Hosono, J. Am. Chem. Soc. **130**, 3296 (2008).

[10] J. M. Luttinger, Phys. Rev. **150**, 202 (1966).

[11] J. Friedel, Philos. Mag. **43**, 153 (1952).

[12] E. M. Lifshitz and L. P. Pitaevskii, *Statistical Physics (Part 2)* (Pergamon Press, Oxford, 2002).

[13] L. P. Gorkov and T. K. Melik-Barkhudarov, Zh. Eksp. Teor. Fiz. (USSR) **40**, 1452 (1961) [Sov. Phys. JETP **13**, 1018 (1961)].

[14] D. Fay and A. Layzer, Phys. Rev. Lett. **20**, 187 (1968).

[15] M. Y. Kagan and A. V. Chubukov, Pis'ma Zh. Eksp. Teor. Fiz **47**, 525 (1988) [JETP Lett. **47**, 614 (1988)]; A. V. Chubukov and M. Yu. Kagan, J. Phys. Condens. Mat. **1**, 3135 (1989); M. Baranov, A. V. Chubukov, and M. Y. Kagan, Int. J. Mod. Phys. **6**, 2471 (1992); A. V. Chubukov and J.-P. Lu, Phys. Rev. B **46**, 11163 (1992); A. V. Chubukov, *ibid.* **48**, 1097 (1993); D. V. Efremov, M. S. Mar'enko, M. A. Baranov, and M. Y. Kagan, JETP **90**, 861 (2000); J. Mráz and R. Hlubina, Phys. Rev. B **67**, 174518 (2003); M. Yu Kagan and V. V. Valkov, ZhETF **140**, 179 (2011) [JETP **113**, 156 (2011)]; A. S. Alexandrov and V. V. Kabanov, Phys. Rev. Lett. **106**, 136403 (2011); S. Raghu and S. A. Kivelson, Phys. Rev. B **83**, 094518 (2011).

[16] A. S. Alexandrov and V. V. Kabanov, Phys. Rev. Lett. **106**, 136403 (2011).

[17] S. Raghu, E. Berg, A. V. Chubukov, and S. A. Kivelson, Phys. Rev. B **85**, 024516 (2012).

[18] C. Platt, W. Hanke, and R. Thomale, Adv. Phys. **62**, 453 (2013).

[19] M. L. Kiesel and R. Thomale, Phys. Rev. B **86**, 121105 (2012); M. L. Kiesel, C. Platt, and R. Thomale, Phys. Rev. Lett. **110**, 126405 (2013).

[20] S. Raghu, S. A. Kivelson, and D. J. Scalapino, Phys. Rev. B. **81**, 224505 (2010).

[21] J. Vucicevic, M. O. Goerbig, and M. V. Milovanovic, Phys. Rev. B **86**, 214505 (2012); M. V. Milovanovic and S. Predin, *ibid.* **86**, 195113 (2012); Oskar Vafek, James M. Murray, and Vladimir Cvetkovic, arXiv:1309.3123; James M. Murray and Oskar Vafek, arXiv:1312.6831.

[22] F. Guinea and B. Uchoa, Phys. Rev. B **86**, 134521 (2012); R. Roldan, E. Cappelluti, and F. Guinea, *ibid.* **88**, 054515 (2013).

[23] See, e.g., B. Valenzuela and M. A. H. Vozmediano, New. J. Phys. **10**, 113009 (2008); I. Martin and C. D. Batista,

Phys. Rev. Lett. **101**, 156402 (2008); T. Li, arXiv:1103.2420; D. Makogon, R. van Gelderen, R. Roldan, and C. M. Smith, Phys. Rev. B **84**, 125404 (2011).

[24] I. T. Dyatlov, V. V. Sudakov, and K. A. Ter-Martirosian, Zh. Exper. Teor. Fiz. **32**, 767 (1955) [Sov. Phys. JETP **5**, 631 (1957)]; J. Polchinski, Nucl. Phys. B **231**, 269 (1984); H. J. Schulz, Europhys. Lett. **4**, 609 (1987); I. E. Dzyaloshinskii, Zh. Eksper. Teor. Fiz. **93**, 1487 (1987) [Sov. Phys. JETP **66**, 848 (1987)]; A. T. Zheleznyak, V. M. Yakovenko, and I. E. Dzyaloshinskii, Phys. Rev. B **55**, 3200 (1997); J. Gonzalez, F. Guinea, and M. A. H. Vozmediano, Europhys. Lett. **34**, 711 (1996); M. Salmhofer, Commun. Math. Phys. **194**, 249 (1998); N. Furukawa, T. M. Rice, and M. Salmhofer, Phys. Rev. Lett. **81**, 3195 (1998); C. J. Halboth and W. Metzner, Phys. Rev. B **61**, 7364 (2000); A.V. Chubukov, D.V. Efremov, and I. Eremin, *ibid.* **78**, 134512 (2008); K. LeHur and T. M. Rice, Annal. Phys **324**, 1452 (2009); Y. Lemonik, I. Aleiner, and V. I. Fal'ko, Phys. Rev. B **85**, 245451 (2012); V. Cvetkovic, R. E. Throckmorton, and O. Vafek, *ibid.* **86**, 075467 (2012).

[25] Rahul Nandkishore, L. S. Levitov, and A. V. Chubukov, Nat. Phys. **8**, 158 (2012).

[26] R. Nandkishore and A. V. Chubukov, Phys. Rev. B **86**, 115426 (2012).

[27] M. L. Kiesel, C. Platt, W. Hanke, D. A. Abanin, and R. Thomale, Phys. Rev. B **86**, 020507 (2012).

[28] Wan-Sheng Wang, Yuan-Yuan Xiang, Qiang-Hua Wang, Fa Wang, Fan Yang, and Dung-Hai Lee, Phys. Rev. B **85**, 035414 (2012).

[29] R. Nandkishore, G.-W. Chern, and A. V. Chubukov, Phys. Rev. Lett. **108**, 227204 (2012); G.-W. Chern, R. M. Fernandes, R. Nandkishore, and A. V. Chubukov, Phys. Rev. B **86**, 115443 (2012).

[30] Gia-Wei Chern and C. D. Batista, Phys. Rev. Lett. **109**, 227203 (2012).

[31] V. P. Mineev and K. V. Samokhin, *Introduction to Unconventional Superconductivity* (Taylor and Francis, Amsterdam, 1999).

[32] J. Gonzalez, Phys. Rev. B **78**, 205431 (2008).

[33] W. Cho, R. Thomale, S. Raghu, and S. A. Kivelson, Phys. Rev. B **88**, 064505 (2013).

[34] P. R. Wallace, Phys. Rev. **71**, 622 (1947).

[35] E. H. Hwang and S. Das Sarma, Phys. Rev. B **75**, 205418 (2007).

[36] A. V. Maharaj, R. Thomale, and S. Raghu, Phys. Rev. B **88**, 205121 (2013).

[37] N. Furukawa, T. M. Rice, and M. Salmhofer, Phys. Rev. Lett. **81**, 3195 (1998).

[38] Rui He, Ting-Fung Chung, Conor Delaney, Courtney Keiser, Luis A. Jauregui, Paul M. Shand, C. C. Chancey, Yanan Wang, Jiming Bao, and Yong P. Chen, Nano Lett. **13**, 3594 (2013).

[39] M. L. Kiesel, C. Platt, W. Hanke, and R. Thomale, Phys. Rev. Lett. **111**, 097001 (2013).

[40] J. Gonzalez, Phys. Rev. B **88**, 125434 (2013).

[41] H. Yao and F. Yang, arXiv:1312.0077.

[42] J. L. McChesney, A. Bostwick, T. Ohta, T. Seyller, K. Horn, J. Gonzalez, and E. Rotenberg, Phys. Rev. Lett. **104**, 136803 (2010).

[43] P. K. Biswas *et al.*, Phys. Rev. B **87**, 180503(R) (2013); M. H. Fischer *et al.*, *ibid.* **89**, 020509 (2014); W.-S. Wang *et al.*, arXiv:1312.3071.

[44] F. Brückner *et al.*, arXiv:1312.6166.

[45] J. C. Nickel, R. Duprat, C. Bourbonnais, and N. Dupuis, Phys. Rev. Lett. **95**, 247001 (2005).

[46] S. Lefebvre, P. Wzietek, S. Brown, C. Bourbonnais, D. Jérome, C. Mézière, M. Fourmigué, and P. Batail, Phys. Rev. Lett. **85**, 5420 (2000).

[47] K. Takada, H. Sakurai, E. Takayama-Muromachi, F. Izumi, R. A. Dilanian, and T. Sasaki, Nature **422**, 53 (2003).

[48] T. Uehlinger, G. Jotzu, M. Messer, D. Greif, W. Hofstetter, U. Bissbort, and T. Esslinger, Phys. Rev. Lett. **111**, 185307 (2013).

[49] Y. Nishikawa, H. Ikeda, and K. Yamada, J. Phys. Soc. Jpn. **73**, 1127 (2004).